Process-Property-Structure relationships in advanced rare earth magnet manufacturing: Towards enhanced performance and developing application

A Dissertation Presented for the

Doctor of Philosophy

Degree

The University of Tennessee, Knoxville

Kaustubh Vidyadhar Mungale

August 2024

ACKNOWLEDGEMENTS

First and foremost, I would like to express my deepest gratitude to my advisor, Dr. Uday Vaidya for his continuous support of my study and research, for his patience, motivation, and the immense knowledge he imparted. His guidance helped me throughout the research and his teachings will stay with me throughout my life. I could not have imagined having a better advisor and mentor for my PhD program.

Besides my advisor, I would like to thank the rest of my thesis committee: Dr. Parans Paranthaman, for his invaluable guidance, insights, and patience with my research and with writing this thesis, Dr. Sudarsanam Babu, and Dr. Claudia Rawn, for their insightful comments and encouragement, but also for the hard questions which incented me to widen my research from various perspectives.

My sincere thanks also go to the Mechanical, Aerospace and Biomedical Engineering Department at the University of Tennessee, Knoxville, the Oak Ridge National Laboratory (ORNL) as well as the Institute of Advanced Composites and Manufacturing Innovation (IACMI) for providing me with all the necessary facilities and resources for the research. I am grateful to Jenny Tate from Tate Industries for supporting this research, and the team members at Fibers and Composites Manufacturing Facility, including Shailesh Alwekar, Vidyarani Hiremath, Pritesh Yeole, Avery Nowlin, Clayton Maner, Vanina Ghossein-Chaya, John Klepzig, Eleni Golloshi, Daniel Locke, Andrew Reed, Sanjita Wasti, Cole Franz, Stephen Sheriff, Surbhi Kore, Hicham Ghossein and Vinit

Chaudhary, for their assistance and for creating a collaborative and supportive environment throughout the years.

I am also indebted to my friends, Digvijay Chauhan, Kaustubh Vibhandik, Asha Shibu, Purva Mallya, Sa'ad Rafie, Kanishka Rawal, Sagar Padghan, Kirtan Davda, Swati Mishra, Samarth Vagal, and Vaikrant Panda for the stimulating discussions, for the sleepless nights, and for all the fun we have had in the last few years.

Last but not the least, I would like to thank my family: my parents Anuradha Mungale and Vidyadhar Mungale, and my brother Chinmay Mungale for supporting me throughout my life and my studies. This accomplishment would not have been possible without all of you. Thank you.

ABSTRACT

This research aims to study advanced rare earth magnet manufacturing, focusing on the structure-process-property relationships that govern their performance and applications. Rare earth minerals are classified as critical materials because they are essential in manufacturing products across numerous cutting-edge technologies including electric vehicles, renewable energy systems, and high-performance electronics.

Bonded magnets are composites with permanent magnet powder embedded in a polymer matrix. Finely powdered (3-300 microns) rare earth based intermetallics such as neodymium iron boron (NdFeB) and samarium iron nitride (SmFeN) are blended with engineering polymers such as epoxy, polyamides (PA6/PA12) and polyphenylene sulfide (PPS), followed by molding the compound to desired shape.

Addition of a polymer binder allows bonded magnets to be produced with low-cost manufacturing methods such as injection and compression molding, whereas sintered magnets are relatively more recourse and capital intensive. Bonded magnets also offer design flexibility and creation of complex shapes with tailored magnetic properties. Despite these manufacturability advantages, the performance of bonded rare earth magnets is limited due to challenges in optimizing the process parameters, material compositions and microstructural properties.

This research preliminarily investigated mechanical, magnetic and microstructural properties of NdFeB powders in a polycarbonate (PC) matrix using multi-phase compounding and compression molding. It is found that with optimum compaction

pressure, high density compounds can be produced. 95% weight fraction magnetic material compounds offered highest maximum energy product [114 kJ/m^3 (kiloJoules per cubic meters)], while 85% weight fraction magnetic material compounds offered highest tensile strength [59 megapascals].

Subsequently, hybrid neodymium-samarium powders with bimodal particle size distribution are studied in a polyphenylene sulfide (PPS) matrix using batch mixing and compression molding. It is found that use of bimodal PSD increases the particle packing density of the compound, thereby increasing the compound density (6.15 g/cc) and maximum energy product [159 kJ/m^3].

Finally, small scale and large-scale additive manufacturing is studied using hybrid neodymium-samarium powders in a polyamide (PA12) matrix. It is shown that additive manufacturing is a competent alternative for bonded magnet manufacturing with compounds produced having maximum energy density of 121 kJ/m^3.

TABLE OF CONTENTS

LISTS OF TABLES

LIST OF FIGURES

Chapter 1

1.1 Motivation

Rare earth magnets are crucial components in several high-tech industries, including consumer electronics, renewable wind energy, solar energy, electric vehicles, automotive, and aerospace. They are a vital part of several devices such as actuators, transducers, sensors, speakers and personal computers. An automobile uses anywhere up to one hundred permanent magnets in starter motors, seat adjusters, wipers etc. [1] Rare earth elements are identified as critical materials by the United States Department of Energy (DOE) [2] as well as the European Commission [3] owing to their relevance in modern technology and the high risk associated with their supply chain. [4] According to the DOE, fundamental research and development needs with regard to magnet manufacturing include driving material development, new process discovery, and demonstrating scalability. [5] This research uses both conventional and advanced processes to develop and characterize various compositions of rare earth based materials for the purpose of expanding the spectrum of their applications.

Neodymium and samarium magnets are the most prevalent types of rare earth magnets owing to their superior magnetic properties and diverse applications. Rare earth magnets exhibit highest strength among all commercially available permanent magnets, up to ten times greater than conventional ferrite magnets.[6] The magnets are intermetallic compounds of the rare earth element, iron and boron and form a tetragonal $Re_2Fe_{14}B$ crystal structure, characterized by a unit cell with three mutually perpendicular axis, four formula units or 68 atoms, and an eight layer repeat structure perpendicular to the *c*-axis.[7, 8] The

high strength of neodymium magnets is because of exceptionally high uniaxial magnetocrystalline anisotropy [H_A ~ 7 tesla (T)] i.e. the material magnetizes along a specific crystal axis. General motors and Sumitomo Special Metals first developed neodymium magnets independently in 1984. [7]

NdFeB are generally classified into sintered and bonded magnets. Until late 1900's, sintered magnets were produced through powder metallurgy. More recently, strip casting techniques are dominating higher grade NdFeB magnets.[9, 10] This is followed by sintering and heat treatment. The precursor for sintering involves conventional powder metallurgy processes. Melt spun microcrystalline material produced by rapid solidification and crushed cast strips are grounded to particles by fine grinding methods like jet milling and cryogenic milling followed by sintering.[11] Advanced techniques like inert gas atomization and hydrogenation disproportionation desorption and recombination (HDDR) are used to produce nanocrystalline phased with specific morphologies. Atomization is used to produce spherical particles, which have lower feedstock viscosity and thus higher flowability in processes such as injection molding. [12]

The powders produced using atomization and HDDR are typically used for making composite bonded magnets. [13] Bonded magnets are composites made of the magnetic powder and a polymer binder. Bonded magnets are cost effective and can be molded into intricate shapes, albeit their magnetic properties are lower since they are not fully dense. Thus, bonded magnets fall in the category called 'gap magnets' which have maximum energy product lying between ferrite (<38 kJm^{-3}) and sintered neodymium (>200 kJm^{-3}).

1.2 Important magnetic properties of permanent magnets

Neodymium iron intermetallics are ferromagnetic, which means that the material is magnetized when subjected to an external magnetic field and remains magnetized after the field is removed. **Remanence** Br(T) is defined as the residual magnetization left behind after the magnetic field is removed. **Coercivity** H_c is the resistance to demagnetization of the magnet. **Maximum energy product** (BHmax) combines these two important properties, remanence and coercivity, and quantifies the magnetic strength of a material. The mathematical definition is stated in the following sections. These properties are represented in a magnetic hysteresis loop. The hysteresis loop and the demagnetization curve are shown in Figure 1-1 and Figure 1-2.

The x-axis represents magnetic field strength H, and the y-axis shows the degree of magnetization I. As an external magnetic field is applied, the ferromagnetic material starts to align its atomic magnetic moment. This is represented by the initial magnetization curve OC shown above and is an irreversible process. The curve approaches an asymptote called the magnetic saturation after which point, further increase in magnetic field has no effect on the magnetization. [14] With the reduction of the magnetic field after this point, the curve follows a different path back along CD. The zero-field intercept (H=0) represents the remanence or residual magnetization. Further application of the magnetic field in the opposite direction follows the demagnetization curve DE. The absolute value of the magnetic field at point E is called the coercivity or resistance to demagnetization H_c. [15]

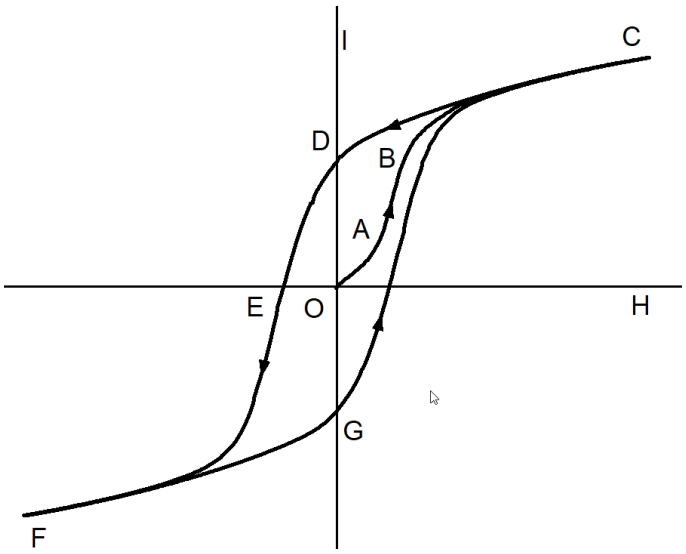

Figure 0-1 Hysteresis loop is a representation of the magnetic force (H) versus maximum flux density (B) of a ferromagnetic material. [14]

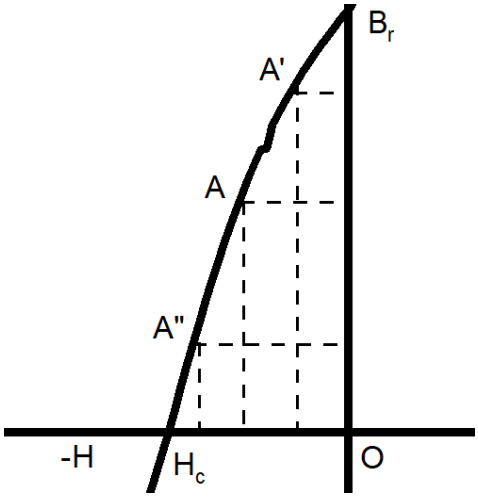

Figure 0-2 Demagnetization curve of a PM is represented by the second quadrant of the hysteresis loop. The curve is used to determine maximum energy product of a magnet. [14]

The second quadrant of the hysteresis loop forms the demagnetization curve B-H. The area formed by the rectangle under working points A, A' and A'' gives the BH value. It has been shown that the effectiveness of a permanent magnet to produce a stray magnetic field in an air gap is given by:

$$U = -\frac{1}{2}\int B.H\ dv \qquad (1)$$

where B is the flux density and H is the remanence over a volumetric element dv. Stray magnetic field is the field channeled outside the magnet and is responsible for the electromotive forces on which magnetic applications rely. [16]

Maximizing or improving BH_{max} or maximum energy product of a permanent magnet, which is a figure of merit in classifying grades as it quantifies the magnetostatic energy a permanent magnet can store. For bonded magnets, $(BH)_{max}$ will depend on the volume fraction and density of the magnet. This relation is shown in Equation 2. [17, 18]

$$(BH)_{max} \propto \left[(1 - V_{non})\frac{d}{d_m}B_r(p)\right]^2 \qquad (2)$$

where V_{non} is the volume fraction of polymer matrix; d is the density of the magnet; d_m is the density of ideal bonded magnet. The volume fraction of the polymer and density achieved after manufacturing decides the maximum energy product. [18] Volume fraction of the non-magnetic phase plays an especially significant role as energy density is proportional to the square of this value. The remanence magnetization is negatively affected during the manufacturing process due to pore volume and internal magnetic shear. [19]

Pores lessen the density of the magnet and internal shear loss is the phenomena caused by isolated magnetic particles interacting with one another in the polymer matrix. Manufacturing parameters such as compaction pressure increase the pore volume and thus decrease the density during the molding step. Dispersion of the particles in the matrix while mixing is important to produce homogenous magnetic compounds. Non homogenous compounds with resin rich areas will lead to inconsistent magnetic field generation.

1.3 Effect of manufacturing process parameters on magnetic properties of bonded magnets

It can be seen in Figure 1-3 that fully dense sintered NdFeB have significantly higher (400 kJm^{-3}) maximum energy product than its counterparts such as samarium cobalt (< 240 kJm^{-3}) or samarium nitride (< 200 kJm^{-3}). [20] Despite the high strength values of sintered magnets, they can only be manufactured in simple geometries and need post processing if the application demands a complex shape. Addition of polymers lowers the magnetic strength by proportion to the weight fraction of polymer added, but offers a diverse portfolio of manufacturing process options. The common trend of research in the bonded magnet field includes improving environmental stability, magnetization, near net shape manufacturing and higher maximum energy product. [21]

Commercial bonded Nd-Fe-B have $(BH)_{max}$ in the range of 80 – 143 kJm^{-3}.[22] Other than intrinsic magnetic properties of the powder and the volume fraction, powder morphology also comes into play in achieving maximum BH_{max} values. An example of two closely related magnetic powders which end up with vastly different energy product after

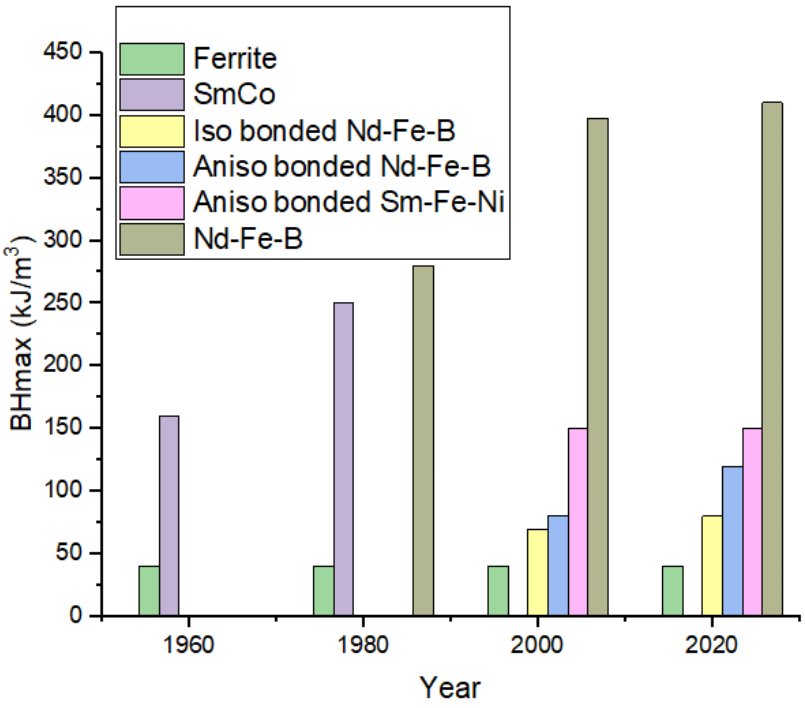

Figure 0-3 BH_{max} evolution over years shows the gains in magnetic strength of various permanent magnets [6]

bonding would be isotropic (MQP) B+ with $(BH)_{max}$ ~143 kJm^{-3}, and isotropic (MQ1) 10–10 with $(BH)_{max}$ ~80 kJm^{-3}, showing the clear effect manufacturing process has on properties. [21] The deterioration of mechanical properties also occurs due to increase in loading fraction of powder. $(BH)_{max}$ is also limited by corrosive environments and thus the binders have to be chosen carefully. The environmental stability can characterized by determining the flux loss or change in the magnetic properties over time at a particular temperature. [21]

There are two types of powders that can be used to make bonded magnets are isotropic and anisotropic. Both powders have nanocrystalline phases but differ in manufacturing techniques and treatments. Hydrogen decrepitation desorbtion recombination (HDDR) along with tempering techniques is used to make anisotropic (Tradename: MQA) grade powders. This process utilizes hydrogen at high temperatures to reduce the grain size to about 0.3 μm. It leads to having more grains per particle increasing coercivity and environmental stability [23, 24] Melt spinning and atomization followed by rapid quenching is used to make MQP (isotropic) powders. Both MQA and MQP are patented by Magnaquench. [25]

Magnetocrystalline anisotropy refers to the phenomenon where a material has an "easy" direction or a preferred direction to be magnetized. This is related to the principal axis of the crystal lattice structure. It is energetically favorable for the material to be magnetized in the direction of one of the axes than the others. An example is shown in Figure 1-4. [14] Magnetic anisotropy is a prerequisite for ferromagnetic materials. Being ferromagnetic,

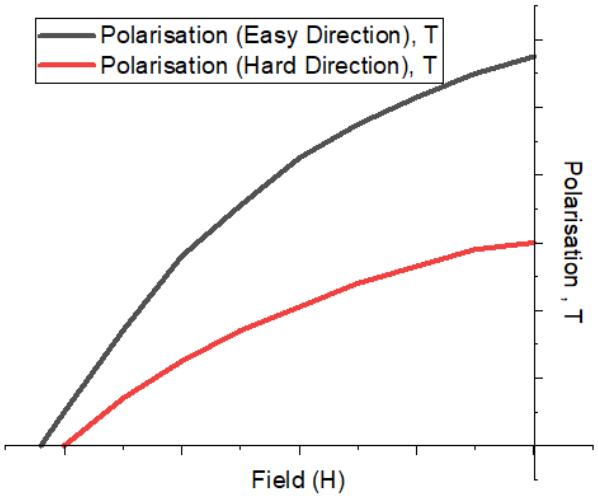

Figure 0-4 Typical demagnetization curves in “Easy” and “Hard” directions demonstrate the intrinsic nature of neodymium magnets to prefer a single direction of magnetization.

neodymium inherently exhibits good magnetocrystalline anisotropy. The arrangement of easy directions within a domain engineered by treatments like tempering under a magnetic field would decide whether the bulk magnet would display isotropy or anisotropy and leads to the above classification. This is called induced magnetic anisotropy. Randomly oriented easy axis are shown in Figure 1-5. The morphological difference in the types is the particle size distribution of the powders.

MQP have a smaller particles size and a narrow distribution. The average size is between 5-25 µm for isotropic while between 100-120 µm for anisotropic. Atomization produces spherical powders which has better flow for injection molding applications. [26] Figure 1-5 models behavior exhibited by MQP powders which have a randomly distributed This research aims to utilize MQP and MQA powders in extrusion bonding and characterize magnetic properties following that. In general, MQA powders have a higher maximum energy density than MQP powders.

Flux loss measurements over time are necessary to determine how the permanent magnet will hold up over time with regard to thermal stability. [13] Flux loss consists of recoverable irreversible loss, structural loss and reversible loss as shown in Figure 1-6, 1-7. They are incurred due to spin relaxation due to corrosion/oxidation with increasing temperatures. Structural losses occur due to rare earth grain boundary phase. [21] Recoverable losses have an inverse proportionality relation with the intrinsic coercivity (H_{cj}). The irreversible losses are related to remanence (B_r) and intrinsic coercivity (H_{ci}) by the temperature coefficients as seen in eqn 3:

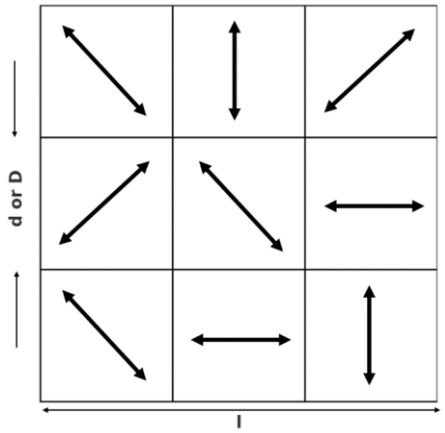

Figure 0-5 Randomly oriented grains with easy axes of anisotropic magnetic material. After magnetization, the grains realign such that the easy axes are oriented in the direction of magnetization, readapted from Chikazumi et. al. [14]

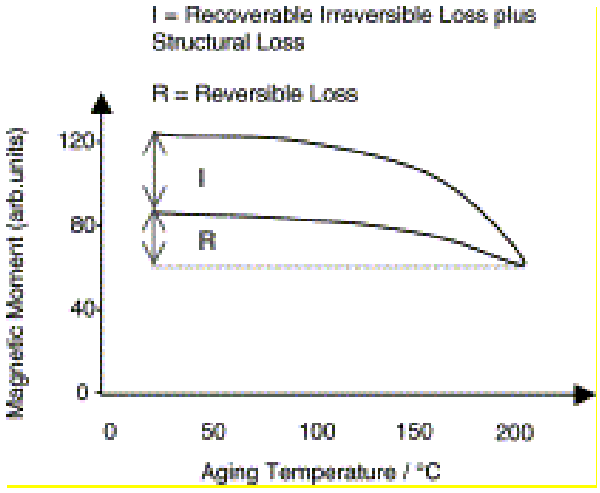

Figure 0-6 NdFeB flux loss at high temperatures shows the loss of magnetic moment with increase in temperature [27]

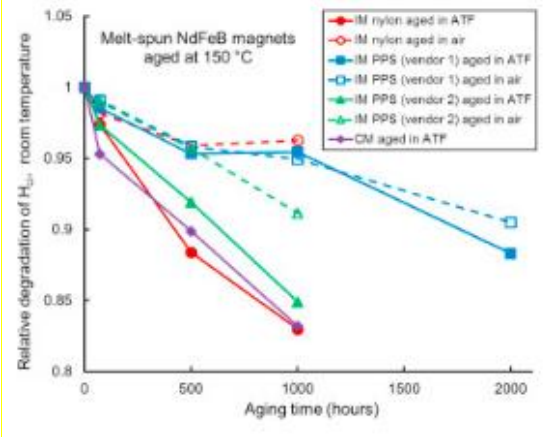

Figure 0-7 Flux losses of several types of MQP grade bonded magnets in PPS and nylon resin manufactured using injection and compression molding [28]

$$\alpha = \left[\frac{(B_{r(T)} - B_{r(RT)})}{B_{r\{RT)} * (T - RT)}\right] * 100\% \qquad (3)$$

where $B_{r(T)}$ and $H_{ci(T)}$ are measured values at temperature T and $B_{r(RT)}$ and $H_{ci(RT)}$ are measured values at room temperature. MQA powders have been shown to exhibit higher flux losses than MQP powders. MQP powders show stability during manufacturing in air.

$$\beta = \left[\frac{H_{ci(T)} - H_{ci(RT)}}{H_{ci(RT)} * (T - RT)}\right] * 100\% \qquad (4)$$

MQA in some instances require processing in inert atmosphere or need special formulated coatings applied to it. [29] Figure 1-8 shows coated MQA powders manufactured using big area additive manufacturing (BAAM) undergoing relatively smaller amounts of flux loses.

Thermomechanical properties play an important role in the alignment of the magnetic particles within a matrix, especially with processes that have a wide range of viscoelastic behavior displayed within the realms of the manufacturing process. This will be true for elastomers and thermoplastic matrices used as binding materials. The viscoelastic behavior, including loss moduli and elastic storage, has been shown to have an effect when the alignment step is being performed. Based on the viscosity at the alignment temperature, the polymer resists the movement of the particles induced by the alignment field. [22, 30, 31] Value of the alignment field applied also has an effect but is mostly dependent on the intrinsic magnetic properties of the powder itself.

In Figure 1-9(a) represents magnetization cure in a 1T alignment field as a function of temperature for Ethylene-vinyl acetate copolymer. The graph in Figure 1-9(b) shows the melting characteristics of the same polymer from differential scanning

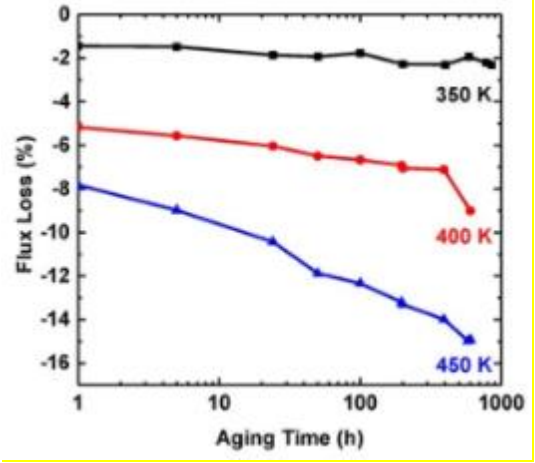

Figure 0-8 BAAM printed MQP-Nylon powders show high amount of flux losses as ambient temperature is increased [32]

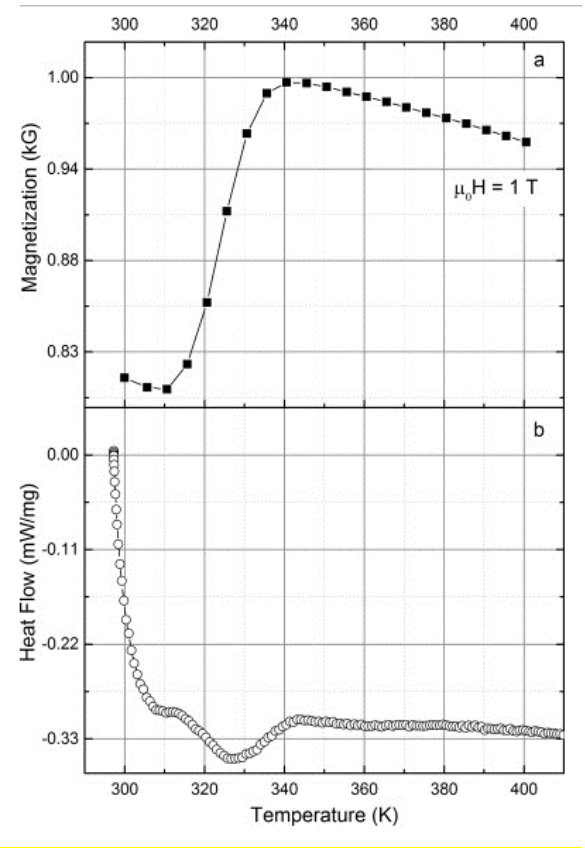

Figure 0-9 Juxtaposition of magnetization and DSC graphs as a function of temperature show that magnetization increases when polymer begins to melt, indicating the low viscosity medium allows the magnetic particles to realign in the direction of magnetization field direction[22]

calorimetry measurements. The onset of magnetization corresponds with the onset of magnetization around 320F, as seen above. Thus, the reduction in viscosity directly corresponds with the increase of magnetization in the sample tested.

Morphologies of the magnetic particles also come into play as the demagnetization behavior inside the grains and at the grain boundary is different thus having a combined effect on the intrinsic coercivity of the bonded magnet. [30] At the same time, loading fraction of the bonded magnets also influences how the particles will move in the viscous melt. Viscous flow of the compound must be carefully optimized when complex techniques like twin screw extrusion are employed to mix the binder and magnetic powder homogeneously. In situ magnetization at die holes (or nozzle heads in case of additive manufacturing), has a great scope for research to improve magnetic properties and cut down the post alignment step.

Thermoset, thermoplastics are used to produce rigid magnets and elastomers are used for flexible ones. Thermoplastics commonly used are polyamides, polyphenylene sulfide, and polyesters while epoxies are used on the thermoset side. Extensive research has been done looking at the suitability of different combinations of resins with permanent magnetic powders. [1, 33, 34]. Figure 1-10 shows the various manufacturing processes practiced in molding magnets. Most commonly used techniques include calendaring, injection molding, extrusion and compression molding.[1] Calendaring is used with elastomers given the nature of the process. Applications with calendaring would include microchip components, micromotors, transmission chip collectors etc. Up to 65% volume fraction is attained by

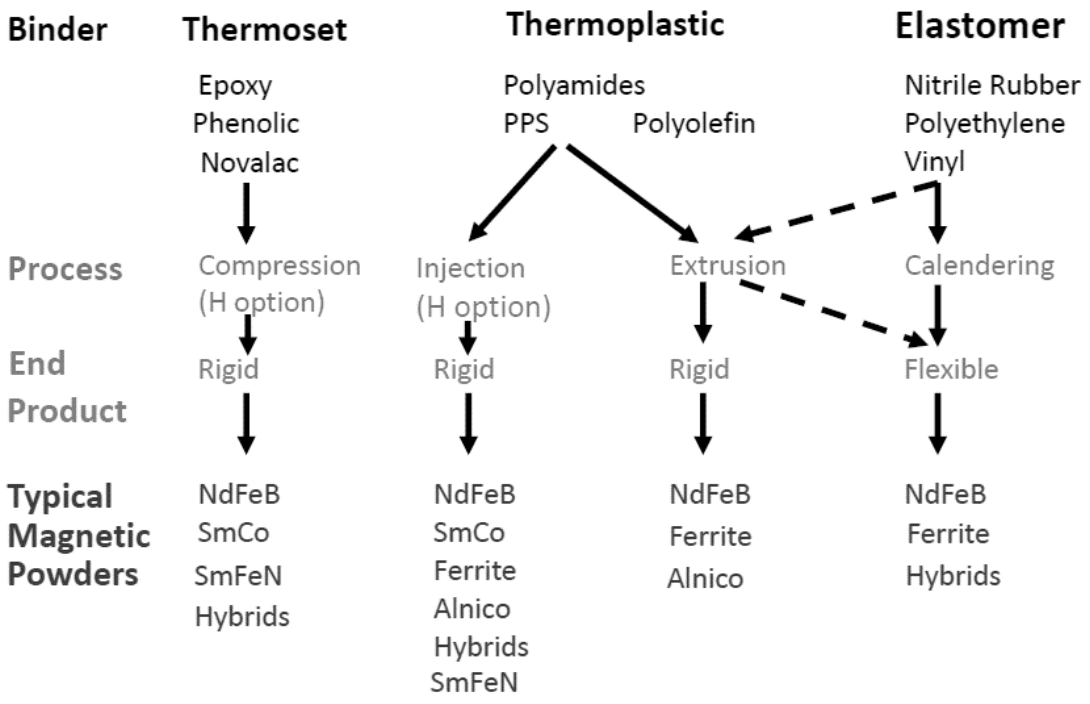

Figure 0-10 Conventional NdFeB bonded magnets production methods as well as feedstock magnetic materials and binders [1]

this process. Injection molding produces precise shape magnets which only require deburring as a post manufacturing operation. PPS and PA6 are engineering polymers used for injection molding/extrusion. Up to 70 % volume fraction is attained using this method. [35] The highest volume fraction, up to 80%, is attained by using compression molding technique with thermoset resins. [35]

Based on the design and performance requirements, bonded magnets manufacturing techniques provide a wide variety of combinations that can be applied to make the magnet. Each process and material come with its advantages and disadvantages. Injection molding allows insert or overmolding capabilities, but the tooling costs are a tradeoff. Compression molding does not require high flowability relative to processes such as injection molding, thus allowing a higher volume fraction magnet production at a low cost but complex geometries are not possible via the technique.

More recently, advanced manufacturing techniques like additive manufacturing have been looked at. Among these, binder jetting [36], fused deposition modeling [22, 32, 37] and direct write printing [38] have been the focus of research. The motivation for additive research has been to produce near net shape parts with minimal post machining while driving the magnetic energy product higher. [37] Fused deposition modeling (FDM) utilizes single screw extrusion process for printing. The aim of the research is being able to produce gap magnets whose BH_{max} values would be over ~15 MGOe. The challenges of this work are in the proper dispersion of the magnetic particles within the matrix. The phenomenon was obvious due to the vastly different energy product values obtained for

the samples tested. [37] There is therefore a need to look at the feedstock pellets made from twin screw extrusion process, which is responsible for proper distribution and dispersion within the matrix.

The objectives of this research aim to employ compounding, compression molding and additive manufacturing processes to optimize the properties of bonded magnets such that they fulfill the gap magnet strength requirements (100-150 kJm^{-3}). The relation between particle-matrix interface and its relation to mechanical properties is also studied. Alternate materials such as using hybrid NdFeB-SmFeN magnetic feedstock with bimodal particle size distribution is studied with the aim of increasing packing density and thereby the magnetic strength of the bonded magnet. The work will integrate analytical tools such as electron microscopy, mechanical and magnetic property characterization and X-ray diffraction to provide a comprehensive evaluation of the samples.

1.4 Research Objectives

This dissertation is comprised of three objectives associated with researching the process-structure-property relations of bonded magnets. Each objective builds on from the last and is consistent with the overarching goal of the study. Brief descriptions of the objectives are given below.

1. Objective 1: Study of small-scale batch mixing, twin screw extrusion and compression molding of neodymium iron boron (NdFeB) particles in a polycarbonate (PC) matrix

Hypothesis: Homogenization during compounding and good interfacial bonding during compression molding will yield magnets with higher density and mechanical properties. The aim of this objective is to gain baseline properties of novel compositions of bonded magnet compounds produced via various matured polymer processing methods. Anisotropic [MQA] bonded NdFeB magnets in a PC binder matrix are fabricated using mixing, extrusion and compression molding process.

The weight fraction of magnetic compounds was iteratively increased while simultaneously optimizing the process parameters. Extruder/mixer residence time, barrel temperatures, screw speed and material feed rate were identified as the key parameters playing a role in subsequent properties of the compound produced. To understand the role played by material composition, various weight fractions (w.f.) of NdFeB/PC on the batch mixer (20, 50, 75, 85 and 95%) are compared to the twin screw extruder with 20, 50 and 75% respectively.

2. Objective 2: Compression molding, small scale and large scale additive manufacturing of bimodal NdFeB/SmFeN high-density magnets in a polyamide matrix

Hypothesis: Use of hybrid NdFeB/SmFeN material as feedstock will improve the packing density and thus the magnetic properties of the bonded magnet because of the bimodal particle size distribution of NdFeB and SmFeN

Influence of process parameters during compression molding and additive manufacturing on hybrid NdFeB/SmFeN nylon (PA12) composite magnets with a bimodal particle size distribution is studied in this objective. Building upon the first objective, which

used NdFeB magnets, the potential of using hybrid NdFeB/SmFeN material with a bimodal particle size distribution (PSD) are studied in this objective. Bimodal PSD has the potential to increase volumetric packing efficiency of the compound by packing the smaller SmFeN (3 μm particle size) in the space between the larger NdFeB (100 μm particle size) powders.

3. Objective 3: *Real world product application of bonded magnets to manufacture electric motor component (rotor) using compression over-molding*

Hypothesis: Manufacturing of rotors can be made efficient with use of a thermoplastic bonded permanent magnet and compression molding

To validate the potential of the technologies studies in previous work, application development is conducted in the manufacturing of rotors using the previously studied advanced manufacturing techniques. In state of art, sintered magnets are used in the application as part of the rotor assembly. Post processing of the sintered magnet is needed before assembly of the rotor system using epoxy as adhesive. Thermoplastic bonded magnets have high potential to cut down the manufacturing step using the process of compression overmolding. A blend of NdFeB/SmFeN hybrid powders in a polyphenylene sulfide (PPS) matrix is overmolded on a 3D printed iron silicon rotor insert and characterized using Vickers hardness testing and optical microscopy.

Chapter 2

1.5 Introduction

As explained in the Chapter 1, Section 1,2, polymer bonded magnets (PBM's) are manufactured by blending of pulverized permanent magnet powders with various polymer systems such as polyamides (PA) [39], polyphenylene sulphide (PPS)[40] and thermoset epoxies[33]. Mechanical characterization of high-density bonded PA and PPS is reported in the literature.[39-41] However, there are a lack of studies on mechanical and magnetic properties of NdFeB in a polycarbonate (PC) matrix. PC is an amorphous engineering polymer with exceptional impact properties. PC has a glass transition temperature of 145^0C, where it softens, and it flows at 155^0. Liu et al. [42] explained that NdFeB magnets have a low impact toughness and often result in chipping, cracking, fracture and thus production losses.

For expanded used of bonded magnets in industry, it is essential to benchmark basic mechanical and magnetic properties of high-performance engineering polymers such as PC. In this work, magnetic PC compounds were manufactured using different types of compounding equipment such as batch mixer and twin screw extruder, compression molding technique, and characterized for their mechanical, magnetic and microstructural properties.

1.6 Manufacturing process methodology of NdFeB bonded magnets

Two types of compounding equipment- a low volume (100 – 200 g) lab scale batch mixer (Brabender Plasticorder W50) and a high throughput (10 kg/hr) twin screw extruder (Berstorff Z25) were employed for melt processing and compounding. Compounded

extrudates were compression molded into flat plates using the Carver 30 Ton Model #3895 hydraulic press. Figure 2-1 illustrates a representative process flow of the manufacturing steps.

Extrusion grade polycarbonate (PC) Lexan resin with density of 1.2 g/cm^3, Magnequench ansistropic NdFeB powder with energy product of 38 MGOe (MQA) produced by Magnet Applications having density of 7.6 g/cm^3 were used throughout the work. PC is dried for three hours at 80 °C in an oven before processing.

1.6.1 Brabender batch mixer

The Brabender batch mixer comprises of a 'mixer bowl'[43] with two counter-rotating blades, as seen in Figure 2-2. The mixer bowl has a free volume of 55 cm^3 and is surrounded by two walls. A temperature control system is used to program the heat setting of the walls and mixer bowl, allowing three zonal settings. The melt temperature for PC is determined to be 155°C. For melt processing of lower magnetic loading fraction (20%, 50% w.f.), a uniform setting of 180°C is used across the three zones. For higher loading fraction (75% - 95% w.f.), the zonal temperatures are raised to 220°C to ensure proper melt flow, given the low amount of polymer in the mixture. The mixer bowl and walls are heat soaked for one hour before beginning the melt processing. The mixer bowl is purged with nitrogen gas via a movable arm and an inner channel that opens at the top of the mixer bowl. An inert atmosphere is necessary to prevent magnetic powders from degrading. The arm in its closed position encloses the mixer bowl entirely allowing a continuous nitrogen flow and enabling inert atmosphere processing. The mixer blade speed is set at 40 rpm and

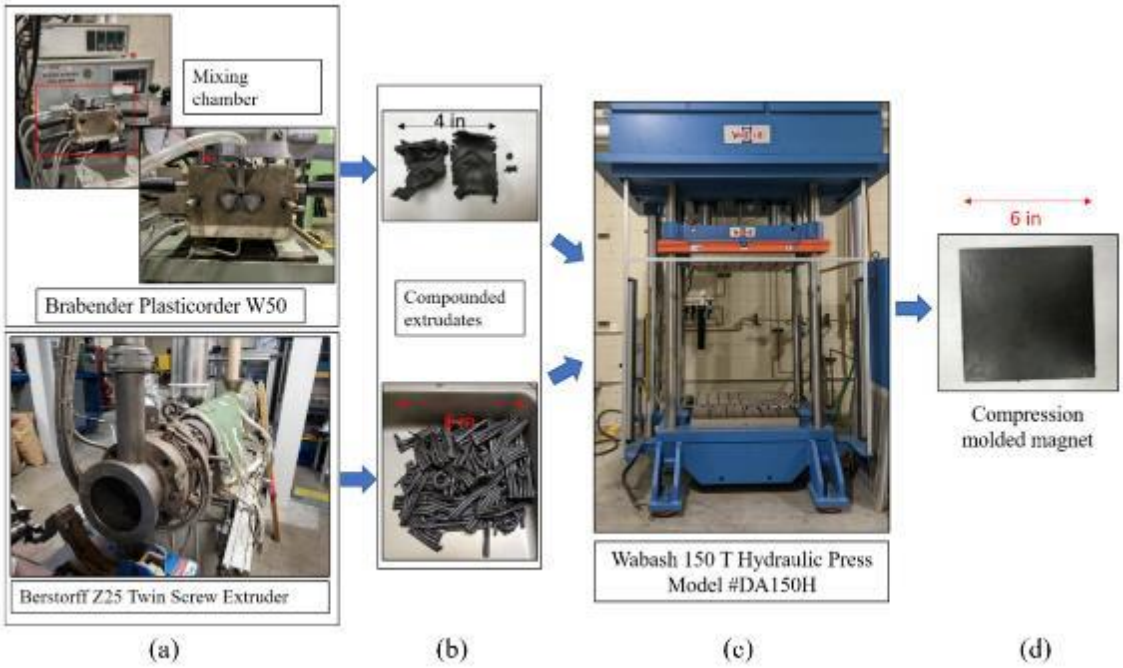

Figure 0-1 (a-b) Batch mixed and TSE extrudates for compression molding (c) 150 Ton Wabash compression molding machine (d) Compression molded NdFeB magnet.

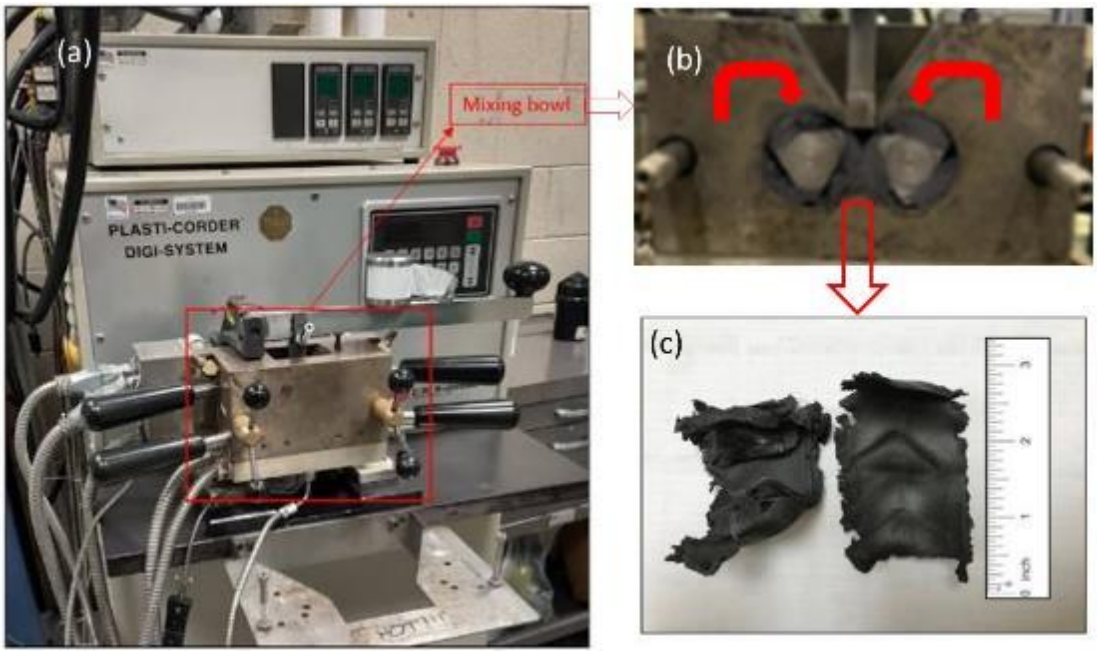

Figure 0-2 (a) Assembly of Brabender batch mixer (b) Enlarged cross-sectional view of mixer bowl with two counter clockwise rotating blades (c) Image of mixed batch ready to be compression molded.

neat PC is added to the mixer bowl. Typical melt processing conditions of 95% w.f. MQA NdFeB/PC magnet in a batch mixer is reported in Table 2.1. The magnetic powder is added in batches when polymer in the chamber has melted, usually after one minute of adding the polymer. Magnetic particles are added in small batches (50 g) to minimize wear on the blades and to avoid over-torquing the motor. The blade speed is increased to 60 rpm at this point for effective dispersion of the magnetic powders within the matrix. The 50 g batches are typically separated by two minutes each or until a uniform melt is achieved and minimal unmixed powder is visible in the mixer bowl.

1.6.2 Twin screw extruder

Berstorff Z25 twin screw extruder (TSE) is used in this work. The TSE has a screw of length 1200 mm as shown in Figures 2-3 and 2-4. The diameter of the screws is 25 mm, center to center distance of screws is 21.5 mm and the length by diameter (L/D) ratio is 48. It is comprised of nine modular barrel elements enclosing the screw. The terminal barrel element (#9) is attached to a four-hole die with hole diameter of 2.4 mm. The barrel elements and the die are heated with cartridge heaters and a temperature control system. Zonal temperatures for compounding NdFeB/PC are shown in Table 2.2. Each zone in the table below represents one modular barrel element.

Temperature at the feed zone is set at 90 °C and is increased in an ascending order up to the die zone. Like the batch mixer, the TSE is heat soaked for an hour before processing. The PC is added at the feed throat using an overhead K-tron self-calibrating gravimetric feeder. The NdFeB is metered downstream directly into the barrel using a

Table 0-1 Typical melt processing of NdFeB/PC in a batch mixer. The resulting magnet product is 95% w.f. MQA NdFeB/PC.

Material added (g)	Time between steps	RPM	Temperature (°C)
Polycarbonate (10 g)	0:00	40	200
NdFeB (50 g)	02:09.54	60	200
NdFeB (50 g)	02:27.91	60	200
NdFeB (50 g)	1:55.73	60	200
NdFeB (40 g)	2:02.63	60	200

Table 0-2 Zonal temperatures (°C) used for compounding MQA NdFeB/PC on a TSE.

Zone 1	Zone 2	Zone 3	Zone 4	Zone 5	Zone 6	Zone 7	Zone 8	Zone 9	Die (°C)
90	110	150	170	180	190	200	205	210	215

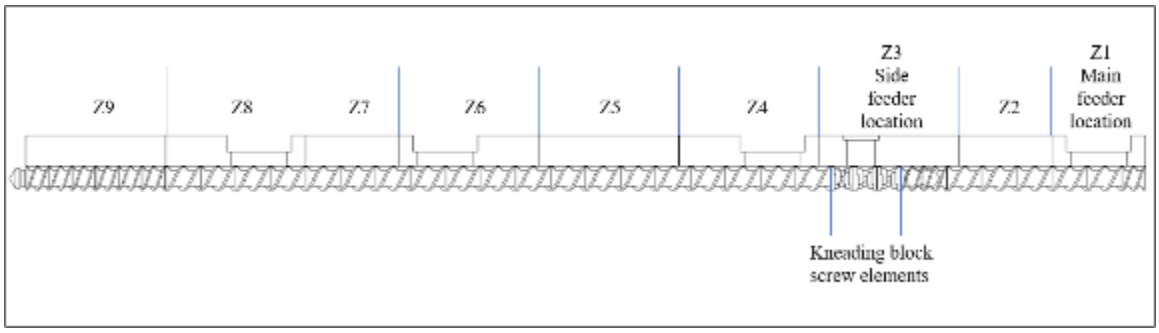

Figure 0-3 Low shear screw design with modular barrel elements, modular screw elements and side feeder location of Berstorff Z25 TSE. Total screw length from Z1-Z9 is 1200 mm [Drawing made using ScrewCon2 software by Berstorff].

Figure 0-4 Image of TSE used with barrel zones and die plate highlighted.

K-tron KT-20 twin screw gravimetric feeder. Side feeder was placed downstream to allow the PC to attain melt flow when magnetic powders were introduced to the process. The feeder screws are enclosed by a discharge tube attached to a side port on barrel element #4. The modular twin screw elements of up to zone 4 are conveying block elements. At zone 5, one zone downstream from when the magnetic powder is introduced, a block of three kneading elements is used for dispersing the magnetic powder in the matrix. All the elements following the kneading blocks until the terminal zone are conveying elements. The screw is designed for low shear to minimize screw wear due to the large particle size distribution (100 - 150 μm) of the NdFeB magnetic particles.

The details of weight fractions of the composite magnets produced with the corresponding feed rates are listed in Table 2.3. Feed rates were reduced as weight fractions were increased because a single flight of the twin screw cannot hold a large volume of high-density magnetic powder. Attempts to use higher feed rates led to high torque on the motor and stopped the extruder.

Other extruder parameters are given in Table 2.4. The speed is decreased for magnetic higher weight percentage runs for a consistent process flow. A pressure transducer reports instantaneous melt pressure at the die plate. It is maintained below 6.89 MPa (1000 psi) for all the runs. The default emergency stop is activated at 22.06 MPa (3200 psi). It is important to keep note of the melt pressure throughout the trial run as it can be used as an indication of steady compound throughput.

Table 0-3 Weight fractions and feed rates for compounding MQA NdFeB/PC on a TSE.

Weight fraction (%)	Polymer feed rate (g/min)	Side feeder rate (g/min)
20	140	50
55	50	60
77	20	70

Table 0-4 Extruder parameters for compounding MQA NdFeB/PC on a TSE.

Extruder Speed	250 rpm (20% & 50% w.f.) 125 rpm (70% w.f.)
Melt pressure range at die plate	3.79 – 6.20 MPa (550-900 psi)
No. of open die holes	4
Die hole diameter	3.2 mm

1.6.3 Compression molding

Compounds produced on the Brabender as well as the TSE were compression molded using a 30-ton Carver hydraulic press. The press has a temperature control system for upper and lower platens with a maximum temperature of 360 °C. A steel tool that produced a flat plate of size 15.24 x 15.24 cm (6 x 6 in) was used for molding low weight fraction (20 – 85%) compounds. Higher weight fractions (95%) were pressed by placing compounds between caul plates because minimal flow of the compounds occurred, making use of a tool redundant.

The platens were preheated to 200°C and allowed to soak heat for one to two hours. The surface temperature was monitored using an infrared thermometer. As extrudates were produced on the compounding equipment, they were immediately collected and placed in the press. Pressure was applied differently to low weight fraction and high weight fraction compounds as shown in Tables 2.5 and 2.6. For high weight fraction compounds, pressure was applied in a single step and not with gradual increments as done with low weight fraction compounds.

1.7 Characterization of NdFeB-PC bonded magnets

1.7.1 Mechanical Characterizations

Tensile testing was conducted as shown in Table 2.7. All coupons were water jet cut into dog bone shapes in accordance with the ASTM D638 standard. MTS 858 tabletop system with 25 kN load capacity servo hydraulic load frame was used to perform the tensile tests.

Table 0-5 Compression molding pressure and dwell time parameters for lower weight fraction (20 - 50 %) MQA NdFeB/PC.

Step #	Pressure increments	Dwell time (min)
1	1-ton force set point (SP) on Carver = 0.38 MPa (55 psi)	15
2	3-ton force SP = 1.14 MPa (166.66 psi)	5
3	5-ton force SP = 1.91 MPa (277.77 psi)	5

Table 0-6 Compression molding pressure and dwell time parameters for higher weight fraction (75 - 95%) MQA NdFeB/PC.

Weight fraction (%)	Pressure applied (Single step)	Dwell time (min)
75, 85	10-ton force set point (SP) on Carver = 3.83 MPa (555.55 psi)	20
95	30-ton force set point (SP) on Carver= 11.49 MPa (1666.67 psi)	

Table 0-7 Specifications of Tensile coupons produced.

Compounding equipment	Weight fraction (%)	Number of Specimens	Average plate thickness (mm)
Twin Screw Extruder	20	5	3.18
	50	5	4.74
	70	5	4.59
Brabender	20	5	2.72
	50	5	2.92
	70	5	1.92
	85	5	2.2
	95%	3	3.8

Extensometer (MST 634.11E-125) with 25.4 mm gage length and a crosshead speed of 2 mm/min was used for testing. Water jetting was used to machine samples into dog-bone shape. Dimensions of samples adhered to Type I specifications for all samples except Brabender 95% samples. Brabender 95% had a limited area for extracting samples and thus was machined to according to the SS3 type dimensions.

1.7.2 Scanning electron microscopy (SEM)

The as received magnetic powders from the manufacturer were analyzed using Zeiss Auriga SEM and focused ion beam (FIB) dual microscope. Fracture surface of tensile samples were also analyzed. All samples were gold sputter coated using an SPI module before analyzing under the microscope. The detector acceleration voltage is set at 5kV and the sample working distance is kept at 10 mm.

1.7.3 Thermal characterization

Thermogravimetric analysis (TGA) was performed on two samples of each compound. Sample weight used was 10 mg for 20, 50, 70 % magnetic w.f. compound and 100 mg for 87and 95% w.f. compound. Instrument used for measurements was TA instruments Q-50 TGA. The ramp rate used was 10 °C/min from room temperature to 600°C. Characterization was performed to determine the weight fraction of the sample.

Differential scanning calorimetry (DSC) was used to characterize the melting behavior of PC resin. TA instruments DSC Q2000 was used for the analysis. The heat-

cool cycle was conducted at a ramp rate of 10°C/min from 40 to 200 °C and vice versa. DSC was performed to determine the melting point and processing temperature range.

1.7.4 Magnetic Characterizations

The magnetic properties of compounded and compressed magnet samples are measured using Quantum Design SQUID magnetometer in as compressed molded and after application of 2 T aligning field while heating up to 500 K. The as compounded and field aligned samples' field dependent magnetization at 300 K measured and energy products are determined and compared with starting powder using the company provided specs. Since the most important figure of merit is the energy product (BH_{max}) which is proportional of square of loaded magnet volume, we characterized the highest magnetic volume loaded samples (87 weight % and 95 weight % samples).

1.8 Results and discussion

1.8.1 Thermal Characterization

Figure 2-5 show the DSC results for neat PC, analyzed using a heat-cool cycle. It was found from the heat cycle that the melting point of PC was in the range of 145 – 150°C and the recrystallization starts at 155 °C. The melting point represents the lower limit needed for processing the resin. It was found that barrel temperatures ranging from 180 °C – 220 °C were optimal for processing the resin with magnetic compound. Although 180 °C was sufficient barrel temperature to achieve melt flow in both the compounding equipment for low weight fraction magnetic compounds (20%, 50%), the temperature had to be

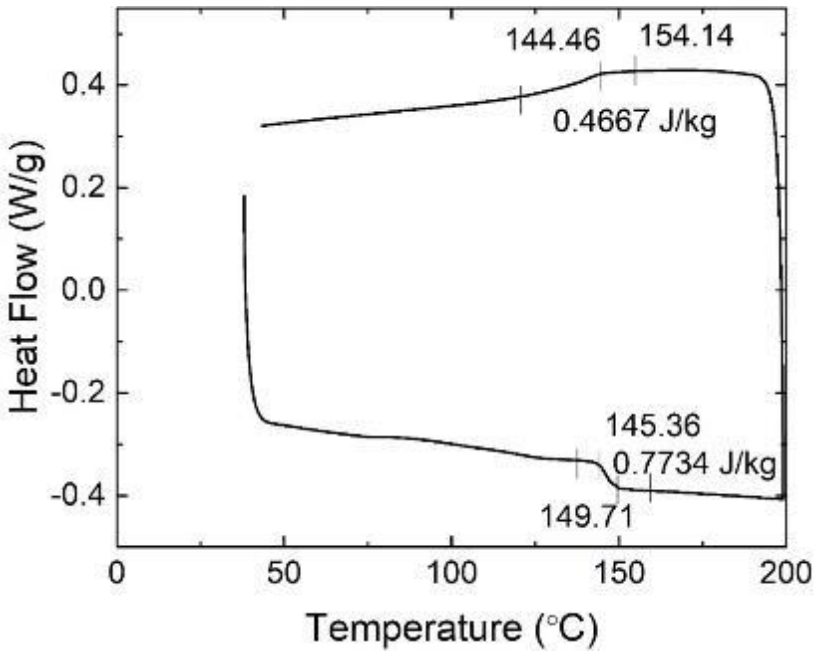

Figure 0-5 DSC analysis for neat PC resin.

significantly increased to 220 °C for higher weight fractions for adequate melt flow.

Figure 2-6. represents the TGA data for 95% NdFeB w.f. sample. It shows the degradation behavior of the PC resin in the compound. The test is performed at a ramp rate of 10°C/min and resin burn off begins in the range of 300-325 °C and ends at 500 °C. The weight of compound lost is recorded and corroborated with the processing weight fraction used. Figure 2-6 shows a resin loss of 4.109% indicating a magnetic weight fraction of 95.89%. Since the test was performed in an inert nitrogen atmosphere, it can be safely assumed that weight at the termination of the test is purely of the NdFeB intermetallic compound.

1.8.2 Mechanical Characterizations

All compounds were tested for tensile properties. Table 2.8 summarizes the properties obtained. For TSE compound properties as seen in Figure 2-7, the stiffness increases with higher magnetic loading fraction. The tensile strength properties, there is an increase between 20% and 50% magnetic loading fraction but a decrease between 50% and 75%. The inferior properties of 20% TSE compound point towards lack of homogenous mixing and are likely a result of porosity formation in the material.

Batch mixed compounds tensile strength improved consistently with increasing weight fraction until 85% magnetic powder loading as seen in Figure 2-8. Tensile strength for 85% w.f. compound was close 60MPa which is only 8% lower than neat PC tensile strength

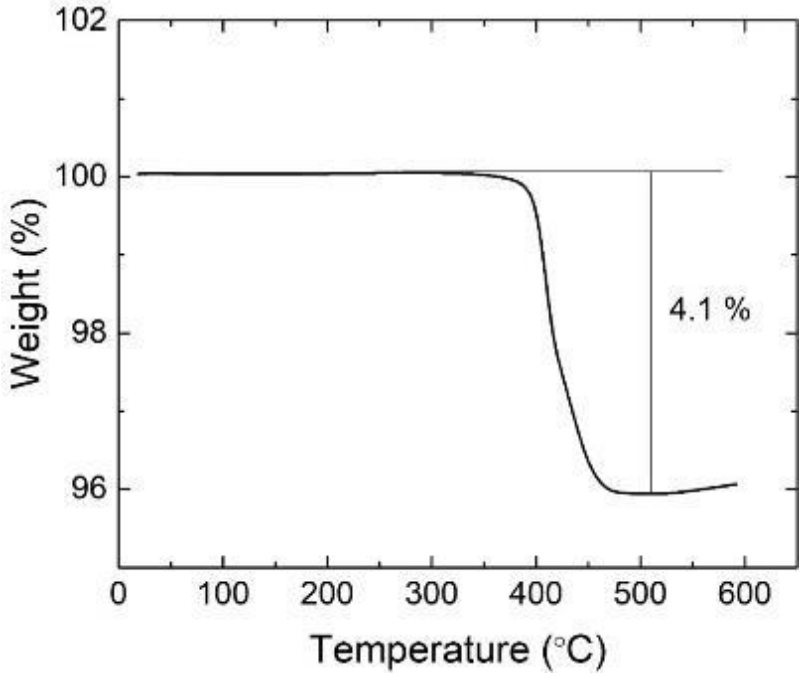

Figure 0-6 TGA graph of 95% w.f. NdFeB compound produced on the Brabender.

Table 0-8 Tensile properties of TSE and batch mixed magnetic compounds.

Sample	Magnetic loading fraction (%)	Tensile Test			
		Strength MPa		Modulus GPa	
		Mean	STD	Mean	STD
TSE	20	37.39	2.08	2.78	0.057
	50	44.35	1.95	3.52	0.078
	75	32.96	5.41	4.09	0.214
Brabender	20	39.45	6.76	2.61	0.032
	50	27.38	12.27	3.36	0.139
	75	51.36	12.66	6.69	0.147
	85	59.25	3.97	9.9	0.104
	95	43.91	3.96	2.26	0.104

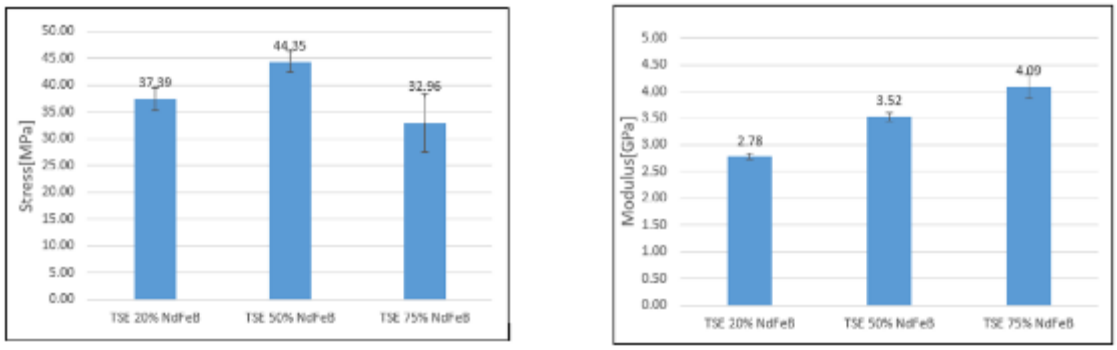

(a) **(b)**

Figure 0-7 Tensile properties of TSE magnetic compounds. (a) Tensile strength, (b) Tensile modulus trend with increasing weight fractions.

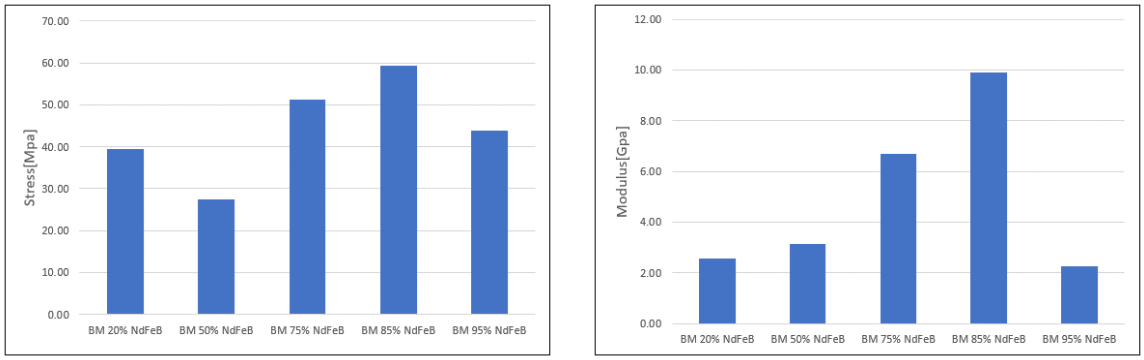

(a) **(b)**

Figure 0-8 Tensile properties of Batch Mixed (BM) magnetic compounds. (a) Tensile strength, (b) Tensile modulus trend with increasing weight fraction.

reported in the material data sheet. The improved tensile strength can be attributed to an optimized bonding strength obtained between magnetic powders and the PC matrix around 85 wt % NdFeB loaded magnets. The same phenomenon explains the high tensile strength of 44MPa obtained for 95% w.f. batch mixed samples.

There is an observed difference in tensile properties between TSE and Brabender samples having the same weight fraction. The low shear screw used in the TSE is not optimized for higher weight fraction compounding. The lack of shear forces do not adequately melt the polymer and mix the compounds efficiently. The batch mixed compounding demonstrates the potential to obtain higher strength with efficient mixing. Thus, further optimization needs to be done to scale up and improve twin screw compounding.

1.8.3 Scanning electron microscopy (SEM)

The SEM image in Figure 2-9 shows the microstructure of the as received MQA NdFeB feedstock powder. The particles have a plate shaped structure and a particle size distribution range of 100-150 µm. Figures 2-10 – 2-12 show the tensile fracture surface of the 20%, 50% and 75% magnetic w.f. compound produced on the twin-screw extruder. It can be observed in Figure 2-10 that particles are dispersed sparsely. Magnetic particles are embedded in the matrix, but the interface between matrix and particles is weak demonstrated by smooth pull off surfaces and clear gaps indicating weak adhesion. Figures 2-11 and 2-12 show the particles are densely packed and are not aligned in the melt

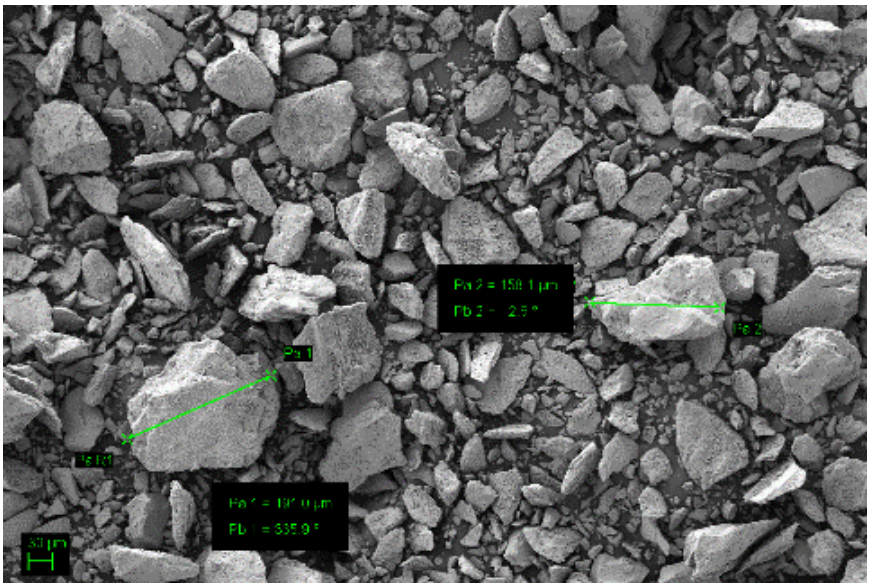

Figure 0-9 SEM micrograph of as received MQA powder

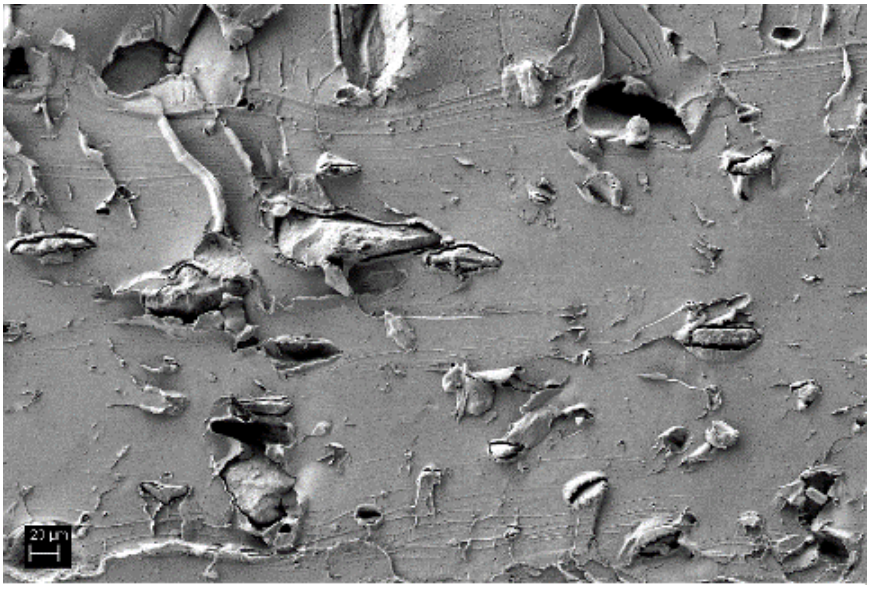

Figure 0-10 SEM micrograph of tensile fracture surface of 20% twin screw extruded compounds showing sparce distribution of magnetic particles

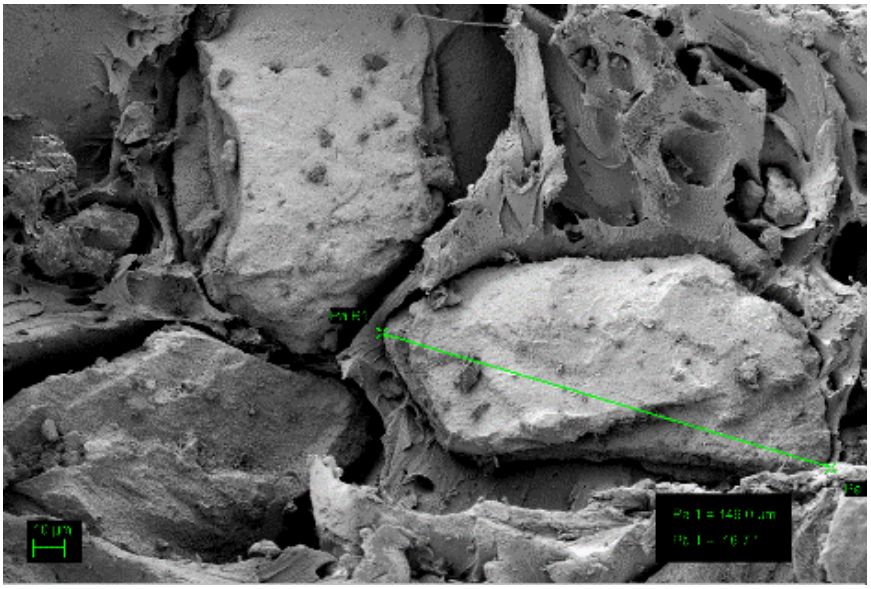

Figure 0-11 SEM micrograph of tensile fracture surface of 50% twin screw extruded compounds showing dense distribution of magnetic particles

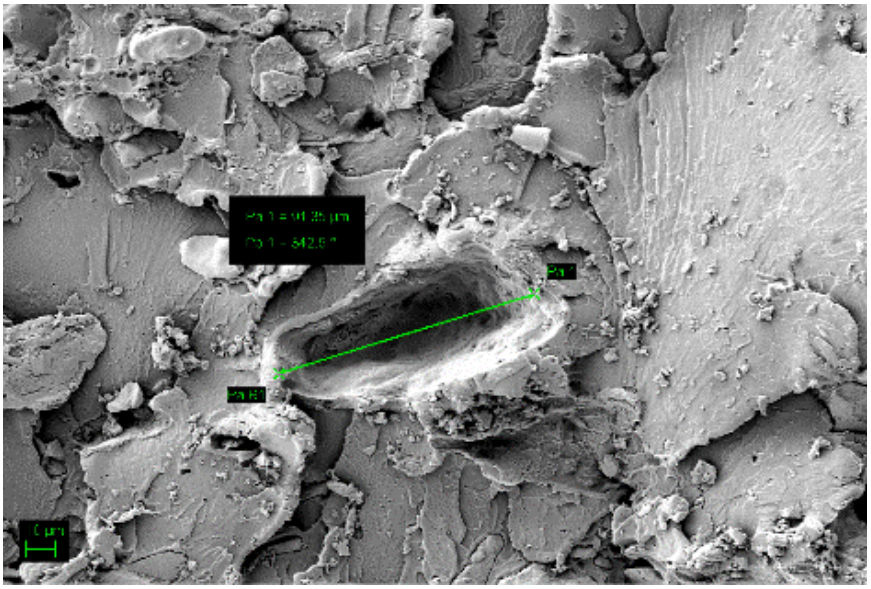

Figure 0-12 SEM micrograph of tensile fracture surface of 75% twin screw extruded compounds showing a crater formed due to particle pull out

flow direction. The matrix is bearing more load and the interfacial surfaces seem to be adhered better than the 20% w.f. compound. Figure 2-13 represents the microstructure of 85 wt. % NdFeB loaded PC-NdFeB composite. A strong adhesive bond can be observed between magnet particles and polymer matrix, supported by the tensile strength data. The bond strength was enhanced through parametric optimization of magnet particle volume, processing temperature and compaction pressure during compression molding.

1.8.4 Magnetic Properties

Figure 2-14 shows temperature profile for the magnetic annealing at 2 T applied field. The measurement samples were mounted in a glass tube inside magnetometer and attained about 80 K higher temperature than softening temperature for the composite to allow the alignment of most of the magnetic particles in the direction of the applied field. Figure 2-15 shows the demagnetization M(H) curve in the second quadrant and the corresponding BH product curves for the 85% and 95% weight percentage loaded magnetic field aligned samples. The 85% w.f. loaded sample exhibits 11.9 MGOe and 95% w.f. loaded sample exhibits 14 MGOe energy product which agrees very well with similar reported literature[1]. If we compare the magnetization surging kinks position in 85% w.f. and 95% w.f compounds, the higher magnetic particle loaded magnet exhibits low temperature rotation than in 85 wt % loaded magnets. This result is consistent with the lower tensile strength observed in higher magnetic particles loaded bonded magnet. High temperature magnetic field alignment of composites and development of anisotropic magnets for the PC-NdFeB magnet is fully optimized.

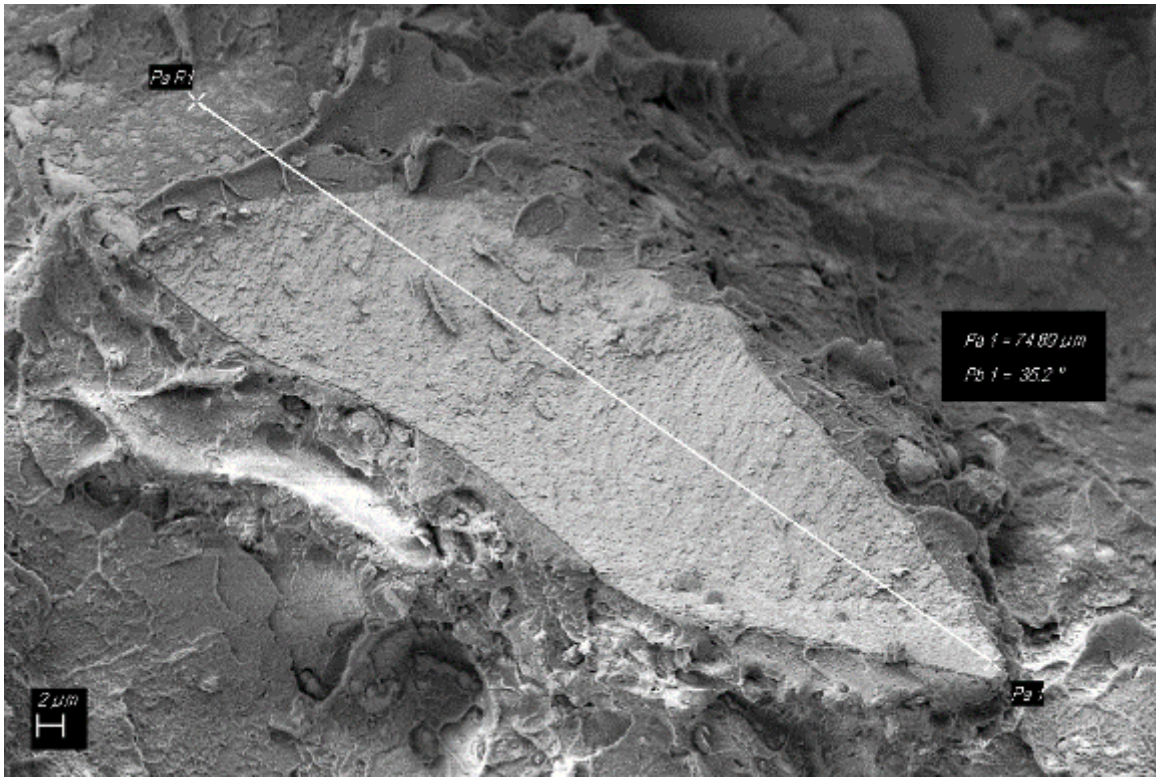

Figure 0-13 SEM micrograph of tensile fracture surface of 85% batch mixed compound showing a particle embedded in the matrix and a strong particle/matrix interface

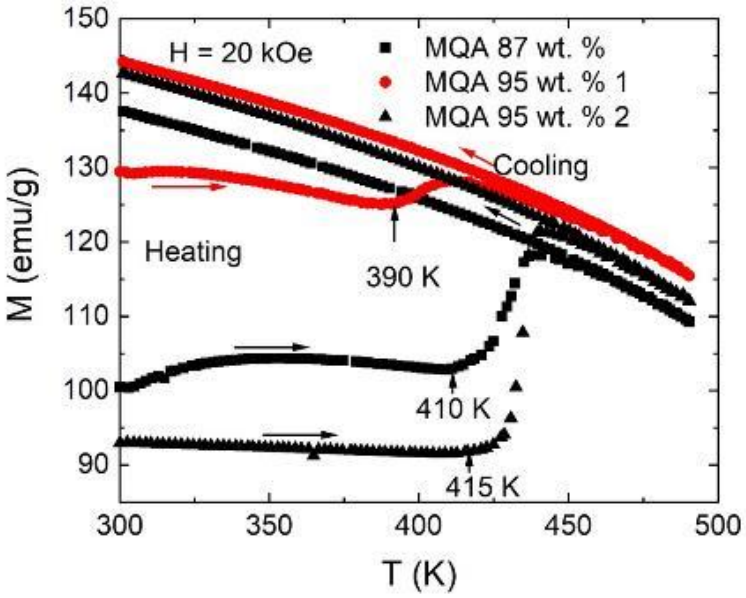

Figure 0-14 Magnetic field heat treatment profile for 85% and 95% weight fraction compounds. The arrows pointing right represent the initial warming M(T) profile and arrows pointing left arrows represent cooling M(T) profile

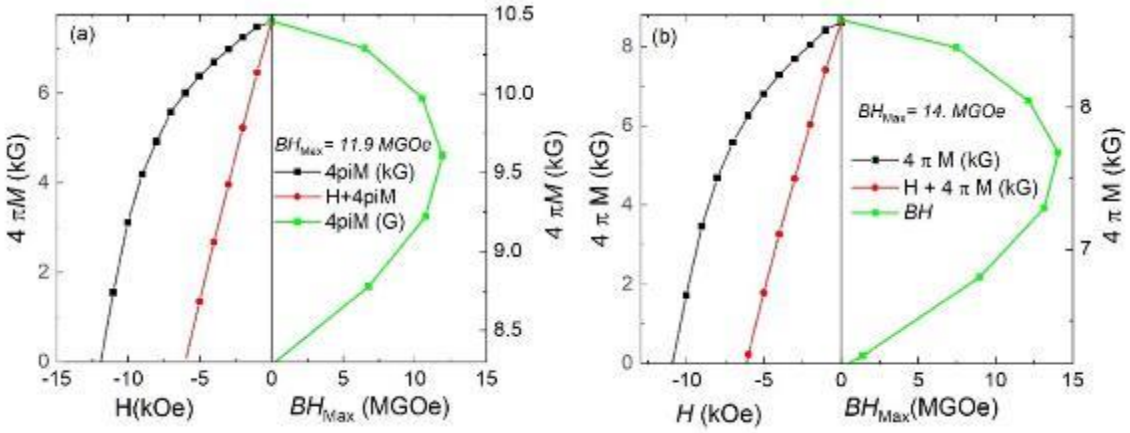

Figure 0-15 Second quadrant magnetization and energy product of the (a) 87 weight % and (b) 95 weight % NdFeB loaded compression molded magnets.

1.9 Conclusion

In summary, PC-NdFeB bonded magnets have been manufactured using melt mixing and compression molding techniques. The mechanical properties, magnetic properties and microstructure has been methodically examined. The bonded magnets demonstrated competitive tensile strength as compared to injection molded nylon- and PPS-bonded permanent magnets. [39, 40]. The melt mixed and compression molded 95 wt. % PC-NdFeB bonded magnet exhibited ultimate tensile strength of 44 MPa for NdFeB loaded magnets, showing potential for growth in various magnetic applications Similarly, energy product of 120.96 kJ/m^3 was achieved in 95 wt. % NdFeB-PC compression molded with post high temperature annealing under 2 T alignment field. From the SEM images of the tensile fractures, excellent bonding was obtained between molded PC matrix and magnetic particle particles with increasing loading fraction. This resulted in higher tensile strength of the NdFeB-PC compression molded magnet. As the advanced manufacturing techniques are maturing, the PC based bonded magnets provide promise as high performance permanent magnets.

Chapter 3

1.10 Introduction to hybrid NdFeB/SmFeN magnets

Chapter 2 studied NdFeB powders in a polycarbonate matrix and the experiments achieved a maximum of 95% weight fraction magnetic compound through compounding and compression molding. It was observed in Chapter 2 (Section 2.4.3) that optimum compaction pressure during compression molding proved to be important for increasing the density and mechanical properties of the compound. It was also observed that polycarbonate, being an amorphous polymer, allows isotropic flow (uniform flow in all directions) in the molten state thus improving microstructural properties such as particle-matrix interfacial bonding. In this chapter, the potential to further increase the magnetic compound density with the use of hybrid neodymium/samarium powders is primarily studied using compression molding. Samarium iron nitride ($Sm_2Fe_{17}N_3$) magnets represent an important class of anisotropic magnets with high magnetic strength (BH_{max}~475 kJ/m^3), curie temperature (476 ºC) and uniaxial anisotropy (K_1=8.6).[44-46]

Hybrid NdFeB/SmFeN magnets have been studied to make bonded magnets and are shown to improve oxidation resistance, corrosion resistance and exhibit higher thermal stability while being cost effective.[47] Rare earth magnet powders have a critical particle size below which the observed coercivity of the material reduces drastically due to oxidation of the Nd-rich phase in the microstructure.[48] SmFeN powders are granulated to sizes in the range of 1-5 µm, whereas anisotropic NdFeB powders with high magnetic strength (BH_{max} ~ 490 kJm^{-3}) typically have a particle size distribution of 100 µm.[19, 49] In hybrid NdFeN/SmFeN bonded magnets, the variable sized powders are mixed to have a

bimodal particle size distribution where the SmFeN particles fit in the voids between larger NdFeB particles hence increasing density of the magnet.[50, 51] According to the Furnaas model of packing, the particle packing density is governed by the volume fraction of coarse and fine particles.[52] The density lowers as the size ratio between coarse and fine particles increases, as shown in Figure 3-1.[52, 53] Thus, to maximize the packing density, the ratio of hybrid powder used has to be optimized. For bonded magnets, the actual volume fraction of magnetic particles (V_{particle}) in hybrid bonded magnets can be estimated based on the density of bonded magnets (ρ_{m}) and magnetic particles (ρ_i), and the mass fraction of magnetic particles (M_i), *i.e.*, as shown in Equation 3.1:

$$V_{particle} = \rho_m \sum_{i=1}^{n} \frac{M_i}{\rho_i} \qquad \text{(Eqn. 3.1)}$$

In this chapter, the following goals are accomplished: (1) Commercially available NdFeB/SmFeN bonded magnets in a polyphenylene sulfide (PPS) matrix are further densified with controlled addition of pure NdFeB powder during the compounding process. The compound is compression molded and its properties characterized using X-ray powder diffraction (XRD), scanning electron microscopy (SEM) and magnetic property measurements. (2) Additive manufacturing is investigated using small- and large-scale processes using commercially available injection molding grade hybrid NdFeB/SmFeN magnets in polyamide (PA12) matrix. The effect of parameters such as

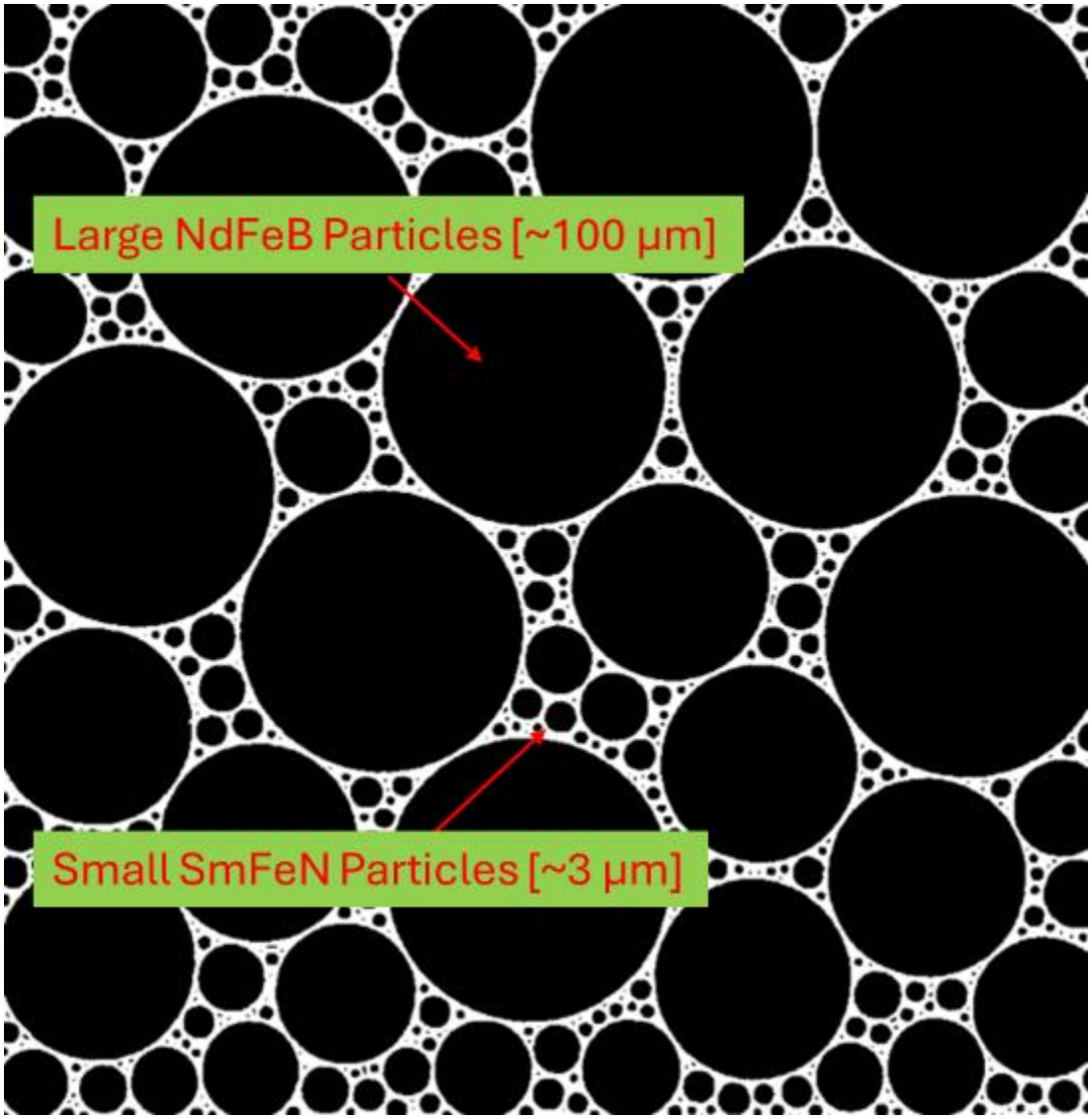

Figure 0-1. Particle packing according to the Furnace model, showing wedges forming between larger particles as size ratio of coarse and fine particles increases (adopted from Myers et. al.) Large particles are representative of NdFeB while small particles of SmFeN in a hybrid bonded magnet

layer height and barrel temperatures on mechanical and microstructural properties are examined.

1.11 Densification of hybrid NdFeB/SmFeN – PPS with compression molding

A blend of anisotropic NdFeB (Magfine) powder and NdFeB+SmFeN PPS pellets (Magfine) MF15P with 93% weight fraction magnetic material are used as feedstock for compounding densified 96% w.f hybrid bonded magnet on the Brabender batch mixer, as shown in Table 3.1. The magnetic properties and mean particle size of feedstock material used is shown in Table 3.2. To achieve the optimized magnetic performance, the ratios of the coarse NdFeB powder and fine SmFeN powder, the content of the binder, and the processing conditions were controlled. The ratio of NdFeB to SmFeB was selected as 3:2 based on the initial packing of as received pellets. The PPS content was reduced from 7% in as received pellets to 4 wt% in the final compound to increase the relative weight fraction of magnetic powder.

The compression molding parameters from Chapter 2, Table 2-6 were adopted for the molding step. The mold temperature was adjusted to the melting point of the PPS binder (280ºC), determined via Differential Scanning Calorimetry (DSC) using a NETZSCH STA449F3 Jupiter thermal analyzer.

1.12 Additive manufacturing of hybrid NdFeB/SmFeN PA12 bonded magnets

Additive manufacturing for bonded magnetic applications offers advantages such as design flexibility enabling tailored magnetic properties, shorter lead times, lower costs by

Table 0-1. Typical melt processing of NdFeB/SmFeN PPS in the batch mixer. The resulting magnet product is 96% w.f. NdFeB/SmFeN-PPS.

Material added	Time between steps (HH:MM:SS)	RPM	Temperature of mixing chamber (ºC)
93% NdFeB+SmFeN PPS pellets (Magfine) MF15P (114 grams)	00:04:00	60	280
NdFeB MF15P (Magfine) powder (86 grams)	00:06:00	60	280

Table 0-2. Magnetic properties and particle size distribution of feedstock material used to compound densified 96% w.f. NdFeB/SmFeN-PPS

Material	B_r (T)	H_{ci} (kOe)	BH_{max} (kJm^{-3})	Mean particle size (µm)
NdFeB MF15P	1.32	14	326.29	100
SmFeN	1.3	10	286.48	3

eliminating need for complex molds, minimizing material waste and ability to integrate multiple components enabling tailored magnetic properties, shorter lead times, lower costs by eliminating need for complex molds, minimizing material waste and ability to integrate multiple components in a single printed structure. Gandha et el. successfully used pellet based Big Area Additive Manufacturing (BAAM) to produce highly dense gap magnets high energy products of ~143.2 kJ/m^3 with use of 70% vol. fraction anisotropic Nd-Fe-B. The limitations include the need for post processing due to large interlayer bead formation, higher void fraction and relatively low mechanical strength (Tensile strength ~14 MPa) most likely due to low interlayer adhesion.[54] It has been shown that injection and compression molded magnets with 65 % magnetic powder fill factors have tensile strengths as high as 50 MPa. Thus, there is a lot of potential to increase mechanical properties of additively manufactured bonded magnets.

This study investigates if optimization of parameters such as layer heights, feed rates and extrusion temperatures in the additive process have the potential to lower the void fraction in a printed bonded magnet. A lower void fraction will thereby increase its density, particle packing, and mechanical strength by improving interfacial bonding between particles and resin. The polymer PA12 is used as a binder during the additive process as it has a lower melting point of 180°C, compared to PA6 (220°C) or PPS (280°C). A small scale Tumaker Pellet Pro and a large-scale robotic extrusion based fused deposition modeling printer is used in the study, as described in Sections 3.2.2 and 3.2.3.

1.12.1 Small scale AM of hybrid NdFeB/SmFeN PA12 printer

The Tumaker Pellets Pro printer, shown in Figure 3-2, was used for the study. The printer is a desktop scale machine with a 3-axis gantry system with a build volume of 290 mm x 180 mm x 200 mm. The Duet 2 Mini 5+ control hardware is used on the machine. The print head consists of a NEMA 23 stepper motor attached to a single screw extruder system comprising of two heater zones and replaceable nozzles. The various nozzle sizes are 0.4mm, 0.8 mm, 2 mm, 4 mm and 5mm. The 2 mm nozzle was determined as the suitable candidate for processing hybrid NdFeB/SmFeN PA12 material and used throughout the study.

The extrusion parameters are optimized in the following order. The heater blocks are of relatively small size (23mm x 16mm x 11mm), thus capable of heating at 5ºC/min. Since the magnetic compound only has 7% wt. fr. binder, the heater temperatures have to be set much higher than the melting point of the polymer to extrude consistently without clogging. The optimized temperatures which did not clog the extruder were determined to be 230ºC at the feed throat and 325ºC at the nozzle. The extrusion rate, measured in motor steps/minute was optimized using E-step calibration (Figure 3-3(a)), where amount extruded by the controller is compared with actual amount extruded, followed by adjustment in extrusion rate if necessary. The feed rate (linear gantry speed) and extrusion multiplier parameters are interdependent. If feed rate is too high, the printed sample has unfilled gaps whereas if rate is too low, over extrusion leads to nozzle blockage and

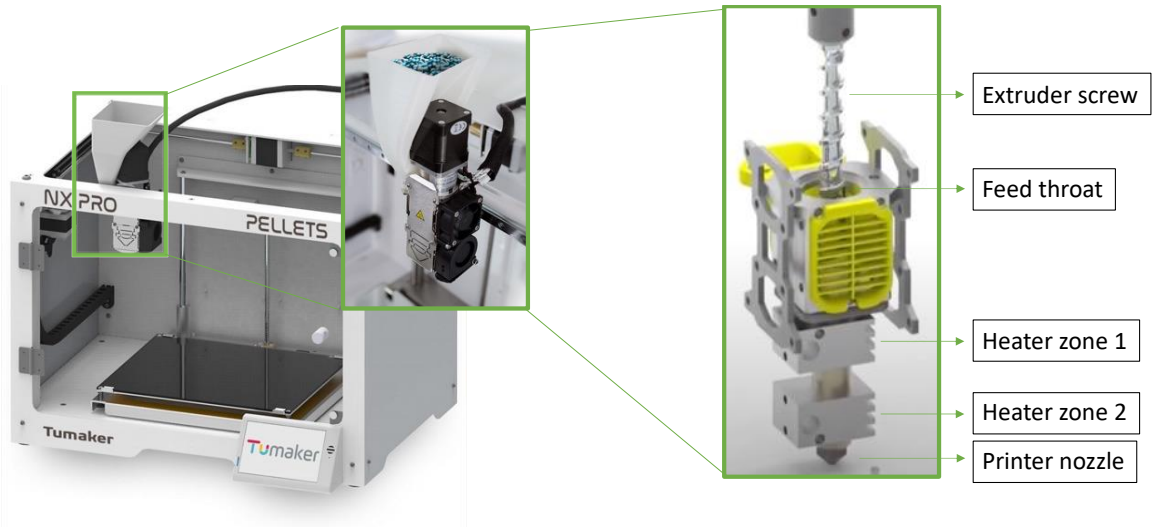

Figure 0-2. Small scale pellet printer with exploded view of the print head extruder assembly. Print head has two heater zones, one close to the feed throat while the other close to the nozzle.

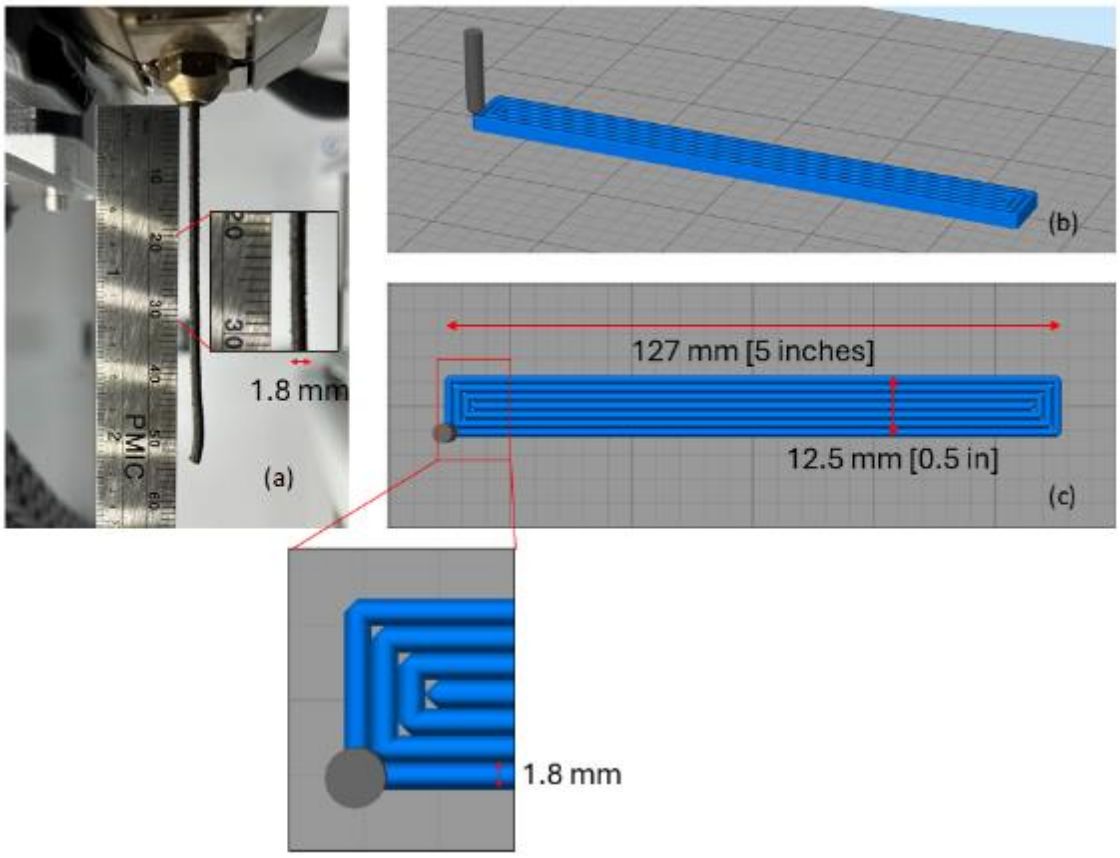

Figure 0-3 (a) Extrudate width consistency and E-step calibration demonstrated. Extrusion width is typically smaller than the nozzle width. Actual width is measured and g-code adjusted accordingly. (b,c) Fill patterns used for parameter optimization where over extrusion or under extrusion is determined

excessive flash on the printed sample. It was made sure that a consistent width was extruded at the nozzle at the beginning of each print. For this study, the feed rate was fixed at 500 mm/min and extrusion inconsistencies were adjusted using the extrusion multiplier parameter. The print bed temperature was set at 70ºC, and first layer height was set 0.1mm higher than layer height to encourage first layer adhesion. The utilized parameters are shown in Table 3-3.

1.12.2 Large scale additive manufacturing-compression molding (AM-CM)

Oak ridge National Lab (ORNL) recently developed the additive manufacturing-compression molding (AM-CM) manufacturing process. Additively manufactured preforms are printed in a mold cavity and compression molded to reduce porosity present due to poor bead to bead interface. The process has thus far focused on fiber reinforced composites. Applying the process to make bonded magnets has the advantage of increasing the magnet density, producing a net shape product, and reducing costs. As seen in Chapter 2, compression molded bonded magnets also have higher mechanical strength and particle alignment in the direction of melt flow.

The additive printing is done using a single screw extruder attached as an end effector of a 6-axis robotic arm. The compression mold is mounted on a platen attached to a linear bearing table which moves in and out of the compression press, as seen in Figure 3-4. The mold platen in moved outside the press for easier accessibility of the robotic arm. The extruder prints the infill pattern directly into the mold cavity, followed by the mold platen being moved into the compression press for molding.

Table 0-3 Optimized process parameters for printing high density bimodal magnet compounds

Tensile coupon printing	Sample 1	Sample 2
Feed rate (mm/min)	500	500
Extrusion rate (steps/mm)	E550	E550
Layer height (mm)	0.20	0.25
Extrusion multiplier	1.35	1.40
First layer speed (relative to default)	100%	100%
First layer height (relative to default)	150%	140%
Bed temp (℃)	70	70
Nozzle temp (℃)	325	325
Extrusion width (mm)	1.8	1.8

The processing conditions for printing the molded magnets were based on previous rheological studies done with the setup. Screw speed is set at 900 rpm, while linear feed rate of 50 mm/s is applied. 7.6 mm nozzle provided the most consistent extrusion width. The nozzle temperature was set at 220ºC while the feed throat was set at 170ºC, while the mold was heated to 120ºC. A 304.8 mm x 304.8 mm (12 in x 12 in) flat plate was produced by using compression pressure of 2777.8 psi (Force- 200 tons) and dwelled for 20 minutes.

Mechanical and magnetic properties were tested for the produced plate with the hypothesis that the AM-CM part will be stronger and denser than parts produced using only additive manufacturing.

1.13 Characterization and Results

Characterization techniques employed were the same as in Chapter 2.3, with the addition of X-ray diffraction (XRD) technique used to analyze phases of NdFeB and SmFeN in the densified hybrid PPS magnets. Any other digressions in characterization methods are noted in their respective sections.

1.13.1 X-Ray diffraction of densified NdFeB/SmFen PPS magnets

XRD data was collected using a PANanlytical X'Pert PRO diffractometer with Co Kα radiation. Rietveld analysis of the XRD data was done performed. The XRD patterns are dominated by the contributions from $Nd_2Fe_{14}B$ and $Sm_2Fe_{17}N_3$ phases beside minor peaks from PPS, as seen in Figure 3-5.

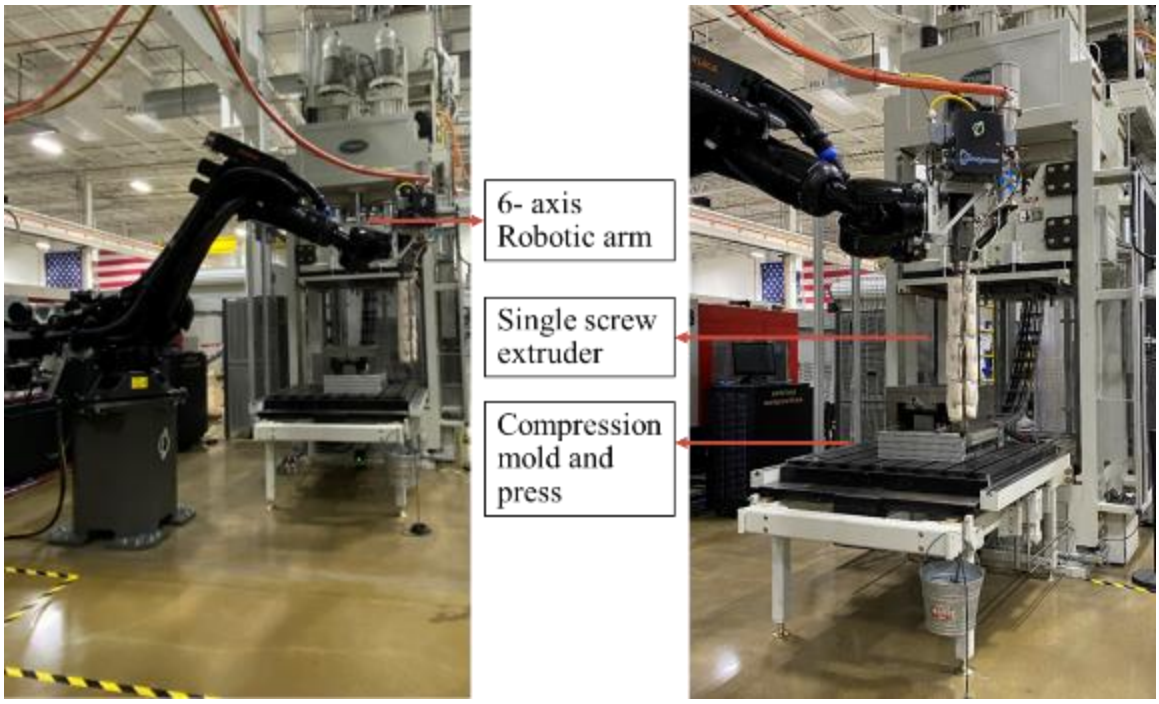

Figure 0-4. Large scale Additive manufacturing-compression molding setup showing the robotic arm, end effector single screw extruder, compression mold and press. The bonded magnet pellets are printed using the extruder end effector directly into the mold cavity. The linear bearings move the cavity into position inside the compression press for the compaction cycle.

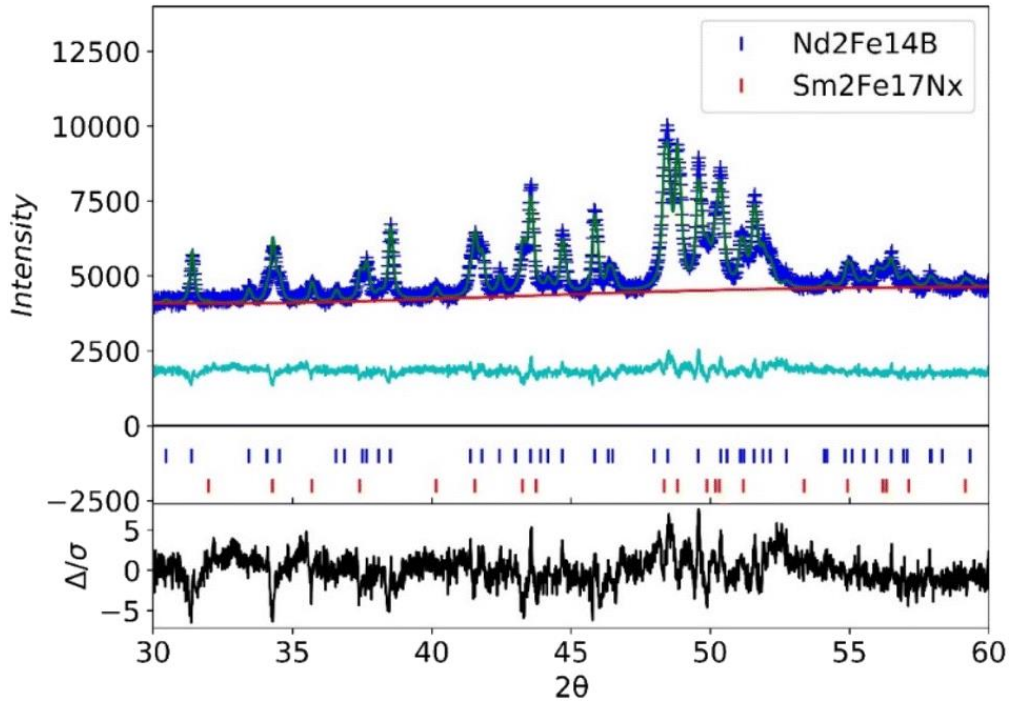

Figure 0-5. Experimental (blue crossing) and fitted (green line) XRD diffraction patterns of the Nd-Fe-B/Sm-Fe-N hybrid bonded magnet indicates the presence of 61% of the Nd2Fe14B phase and 39% of the Sm2Fe17N3 phase, confirming the target set in experimental methodology

Table 0-4. XRD Rietveld-fitted results of the Nd-Fe-B/Sm-Fe-N hybrid bonded magnet. (wR = 2.22%, R = 1.71%, GOF = 1.4)

Phase	**Space group**	**Lattice constant a (Å)**	**Lattice constant c (Å)**	**Content (vol%)**
$Nd_2Fe_{14}B$	$P4_2/mnm$	8.7987 (2)	12.2108	61
$Sm_2Fe_{17}N_3$	*R-3M*	8.7373 (5)	12.6568	39

The Rietveld analysis indicates the presence of 61% of the $Nd_2Fe_{14}B$ phase and 39% of the $Sm_2Fe_{17}N3$ phase, confirming the target set in experimental methodology, Section 3.2. The fitted lattice constants are also in agreement with previous literature. [55]

1.13.2 Mechanical characterization of additively manufactured hybrid magnets

1.13.2.1 Small scale additive manufacturing

Two sets of samples with layer heights of 0.2 mm and 0.25 mm were used and properties from samples were compared. Five specimens of each type of sample were printed, as seen in Figure 3-6. The samples were printed in dog bone shape and flatwise orientation adhering to Type 5 specimen recommendation in the ASTM standard D-638-14. The thickness of all samples was 3 mm, with a one layered outline and rectilinear infill pattern with 100% interior fill percentage. Each layer had a 10º infill angle offset relative to the previous layers, following the pattern -80º/90º/80º to the testing direction. The gauge region of the coupons was printed in the same direction as testing, as it has been shown for the FDM process, the highest tensile strength is obtained if the raster orientation is 0º. [56, 57]

The test was conducted at the rate of 1 mm/min. Yield strength and young's modulus can vary with the orientation, layer height, and build plane.[58] All specimens failed within the gauge length. As seen in Table 3-5, the mean strength value of 0.2 mm layer height (LH) sample was 10% higher (20 MPa) than the values of 0.25 mm LH samples (18 MPa). But the 0.25 mm LH sample had twice the young's modulus compared

Table 0-5. Tensile properties of small scale AM and large scale AM-CM magnetic compounds

Sample	Magnetic loading fraction (%)	AM Layer height (mm)	Tensile Test			
			Strength MPa		Modulus GPa	
			Mean	STD	Mean	STD
Small scale AM	95	0.2	20.10	3.59	0.886	0.102
	95	0.25	17.88	0.928	2.098	0.67
Large scale AM-CM	95	3.3	25.09	1.43	5.49	0.36
Manufacturer data sheet (Injection molded)	95	-	27	-	12	-

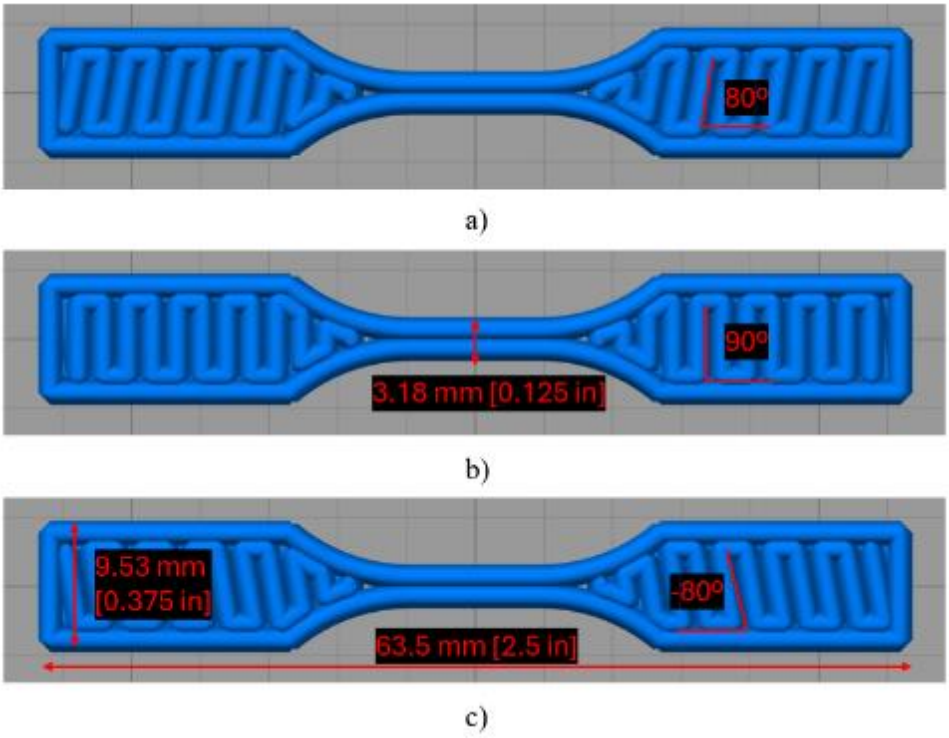

Figure 0-6. Pattern used to print tensile coupons with infill angle offset of each subsequent layer: a) 80º, b) 90º, c) -80º

to the 0.2 mm LH sample. Giri et. al. showed that tensile strength increases with layer thickness until a threshold value, followed by a decline, which explains the drop of strength in 0.25 mm LH samples. [59]

1.13.2.2 Large scale AM-CM

5 specimens were cut using a computer numerical control (CNC) machine from the AM-CM flat plate adhering to Type I of the ASTM D-638-14 standard and tested at a rate of 2mm/min. Machining speeds and feeds were selected such that machined surfaces were smooth and did not have any chips or breaks. The tensile coupons were tested along the print direction (0º) of the manufactured plate. The tensile strength of AM-CM sample was 25% higher than the small-scale printer and only 4% lower than the manufacturer provided data for injection molded magnets. The AM-CM plate had a density of 5.4 g/cm^3 compared to 5.2 g/cm^3 of the small-scale AM samples. The high strength can be explained by better compaction of the material and reduction in porosity as shown by the 4% increase in density. The Young's modulus of the AM-CM sample was significantly higher (2.5 – 5 times) than the small scale AM samples, with a value of 5.49 GPa.

1.13.3 Thermal Characterization of hybrid NdFeB/SmFeN – bonded magnets

1.13.3.1 Differential Scanning Calorimetry (DSC)

As seen in Figure 3-7, it was observed that the melting range of PA12 matrix in the compound was between 160ºC-195ºC, with a peak at 187ºC. The recrystallization

occurs in the range of 135ºC-155ºC. As we noted in Chapter 2-Section 2.4.1, high weight fraction magnetic compounds need to be processed at temperatures much higher than the

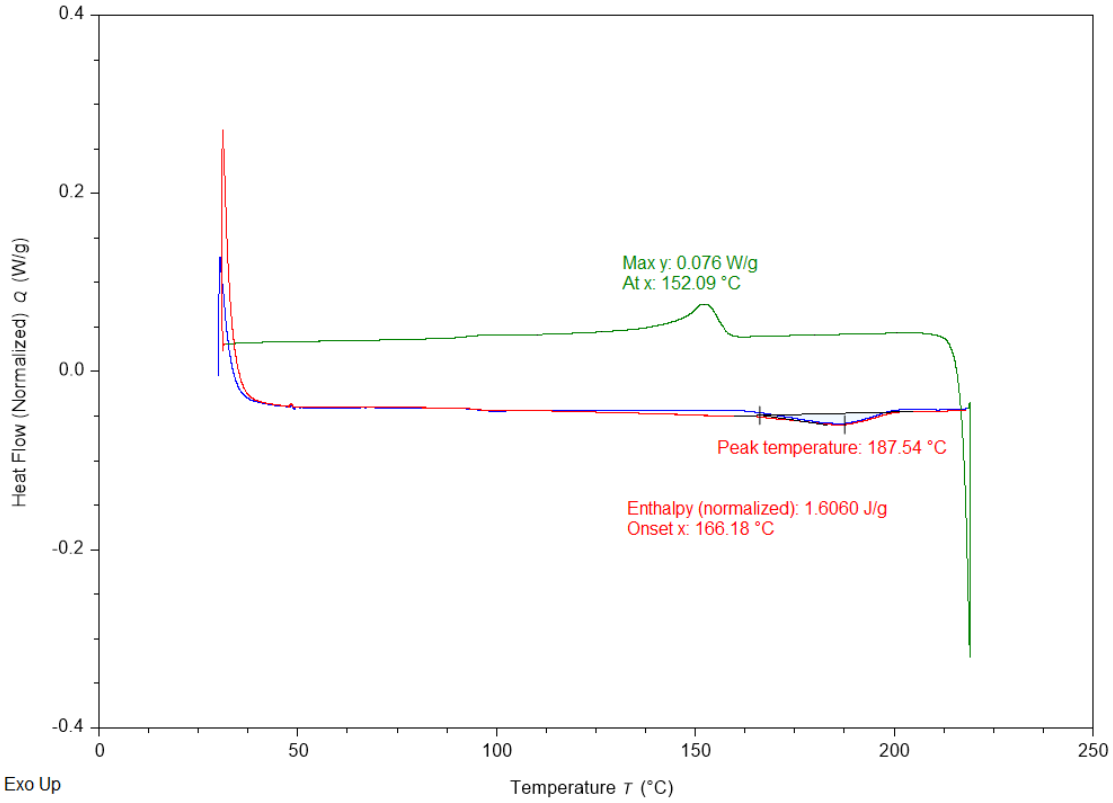

Figure 0-7 Differential Scanning Calorimetry of hybrid NdFeB/SmFeN bonded magnet in a PA12 matrix showing that the melting range of the polymer was between 160ºC-195ºC, with a peak at 187ºC. The recrystallization occurs in the range of 135ºC-155ºC.

melt temperature. Thus, the extruder nozzle in the AM processes was set to 320ºC to avoid material cooling and maintain consistent extrusion width. The feed throat was set to slightly above melting for small scale AM at 220ºC given the small length of the screw and low power of the motor. For large scale AM, the feed throat temperature was set at 160ºC.

1.13.3.2 Thermogravimetric Analysis

The thermogravimetric analysis conducted on hybrid magnetic compound in PA12 matrix can be seen in Figure 3-8. The test was conducted at a rate of 20ºC/min on received pellets, as extruded filament from the printed and the printed sample. All samples confirmed that the weight fraction of the magnetic compound was in the range of 95-95.5%.

1.13.4 Magnetic property characterization of hybrid NdFeB/SmFeN – bonded magnets

The magnetic compounds were tested in a Quantum Design MPMS-3 Vibration Sample Magnetometer (VSM) at various temperatures (300K, 325K, 350K, 375K, 400K).

1.13.4.1 Densified hybrid NdFeB/SmFeN – PPS bonded magnets

The densified hybrid PPS bonded magnets were post-annealed for particle alignment under an external magnetic field of 1.5 T at a temperature of 590K, followed by testing for magnetic properties at 300K, with the hysteresis loop shown in Figure 3-9. The

density of the obtained magnet was 6.2 g/cc, 20% higher than the as received hybrid pellets. Excellent magnetic properties were obtained with B_r of 10.4 kG, H_{ci} of 10.8 kOe, and a

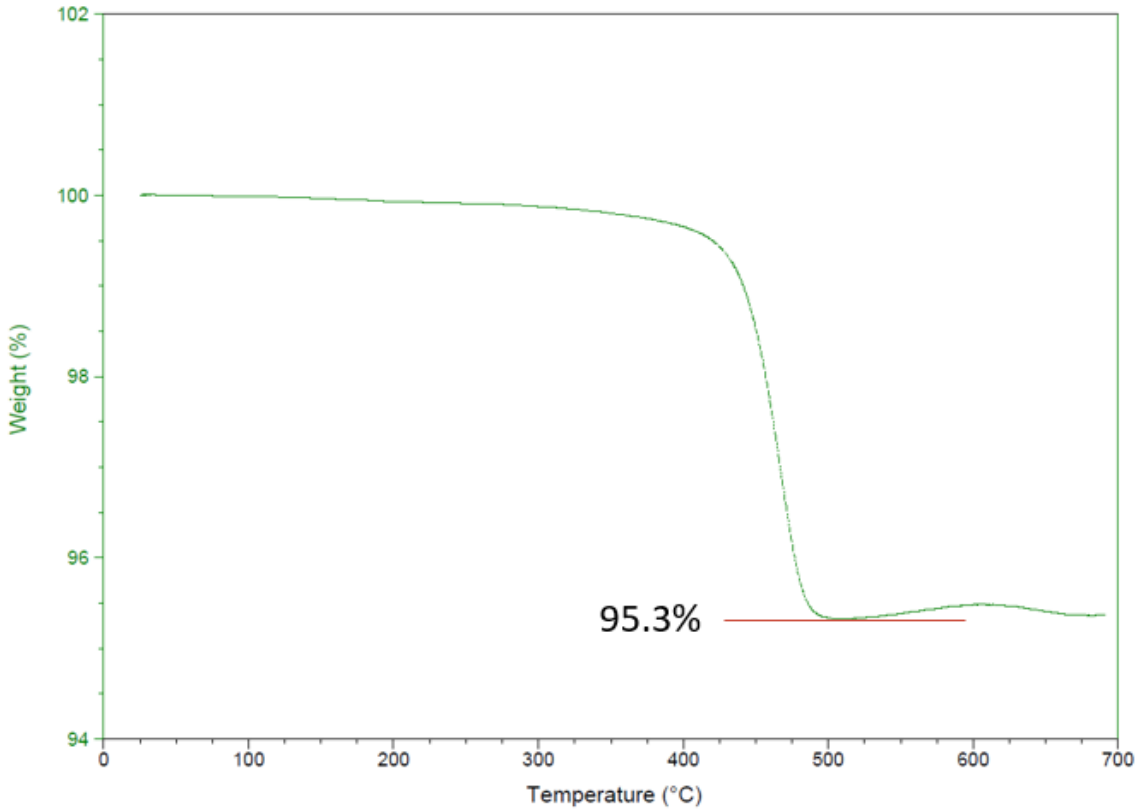

Figure 0-8. The thermogravimetric analysis conducted on hybrid magnetic compound in PA12 matrix shows a magnetic weight fraction of 95.3% and polymer burn off occurring between 400ºC and 500ºC. There is a slight increase in weight after 520ºC likely due to oxidation of the magnetic compound

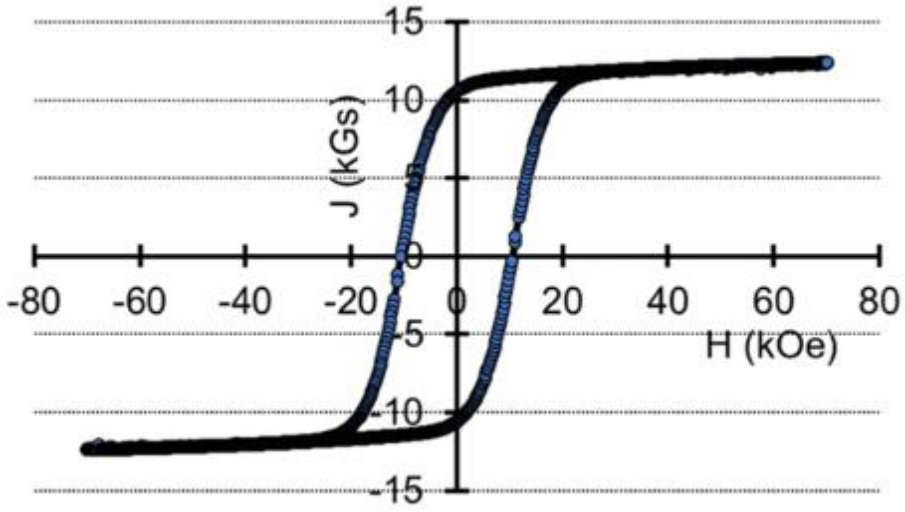

Figure 0-9. Magnetic hysteresis loop J–H of the densified NdFeB/SmFeN hybrid bonded magnet in a PPS matrix showing excellent magnetic properties with with B_r of 10.4 kG and H_{ci} of 10.8 kOe

$(BH)_{max}$ of 159 kJ/m^3. The H_{ci} is slightly higher than that of SmFeN (10 kOe) but less than that of NdFeB (14kOe), resulting from linear overlapping effect and stray magnetic field in the hybrid magnet. The BH_{max} is 39% higher than the 95% w.f. NdFeB-PC studied in Chapter 2, due to the higher packing fraction attained by using the bimodal particle size distribution of the hybrid powders.

1.13.4.2 Small scale hybrid NdFeB/SmFeN – PA12 magnets

Hybrid PA12 AM magnets were post-aligned in the VSM at 300K (room temperature). Figure 3-10 shows the hysteresis of the as printed magnet with randomly oriented particles along with the post alignment magnet under an applied magnetic field of 1T. A significant increase in magnetic strength is obtained after alignment, with the post-alignment magnetic properties B_r of 9.48 kG, H_{ci} of 10.65 kOe, BH_{max} of 124.14 kJ/m^3 and an 89% degree of alignment. The density of the magnet is 5.207 g/cc. Figure 3-11 shows the hysteresis loops of the post aligned sample performed at higher temperatures of 325K, 350K, 375K, and 400K. It is observed that remanence and coercivity of the sample linearly decreases with the increase in testing temperature.

1.13.4.3 AM-CM hybrid NdFeB/SmFeN – PA12 magnets

The random and post alignment hysteresis loop is shown in Figure 3-12. with the post-alignment magnetic properties B_r of 8.5 kG, H_{ci} of 11.05 kOe, BH_{max} of 116.18 kJ/m^3. There is a 9% decrease in the BH_{max} value compared to the small scale AM sample most

likely due to the selected specimen having non uniform particle alignment leading to a lower remanence. The coercivity on the other hand is 5% higher than the AM only sample.

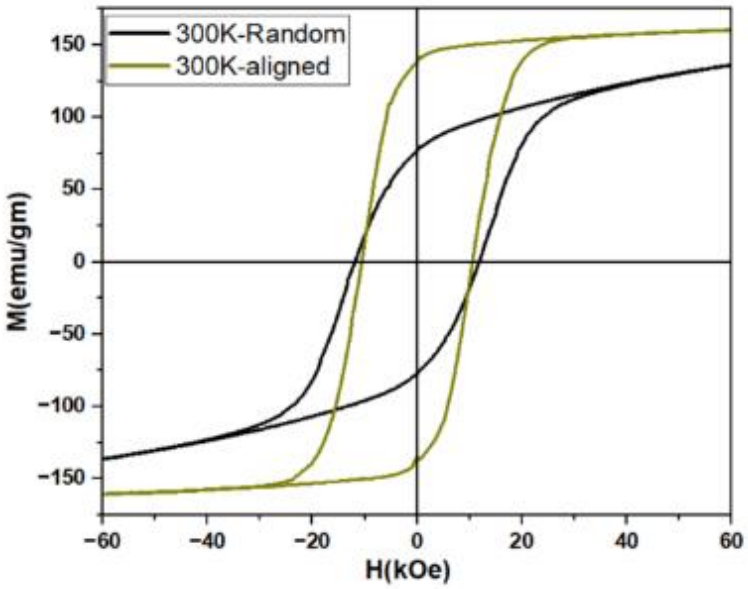

Figure 0-10. Hysteresis loop of as-printed (300K – Random) and post aligned (300K – aligned) small scale hybrid NdFeB/SmFeN PA12 magnets. As expected, once aligned, the remanence value increases almost two fold. The saturation magnetization is attained at a lower field strength as well.

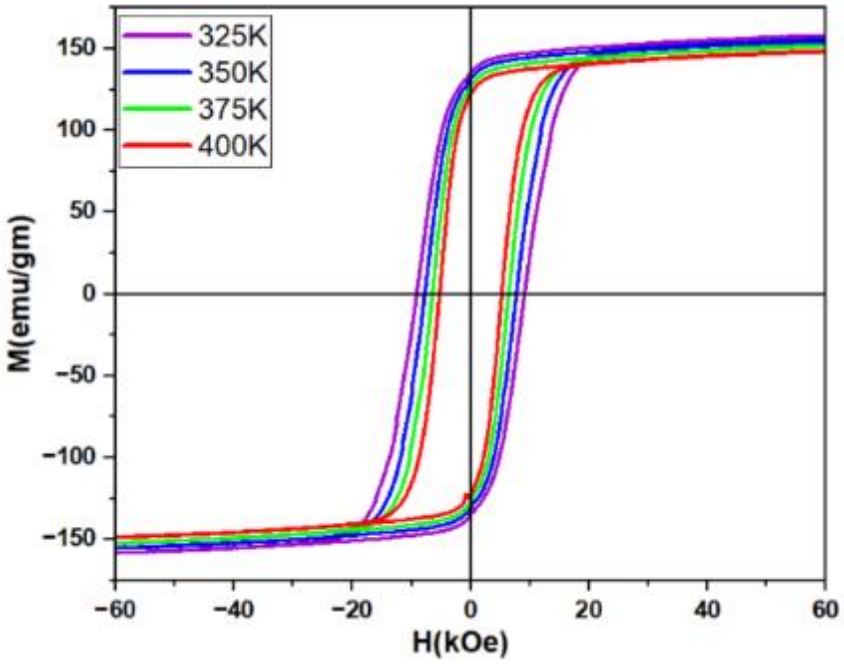

Figure 0-11. Hysteresis loop of post aligned small-scale hybrid NdFeB/SmFeN PA12 magnet at higher temperatures (325K, 350K, 375K, 400K). There is a steady decrease in magnetic properties with increasing temperatures.

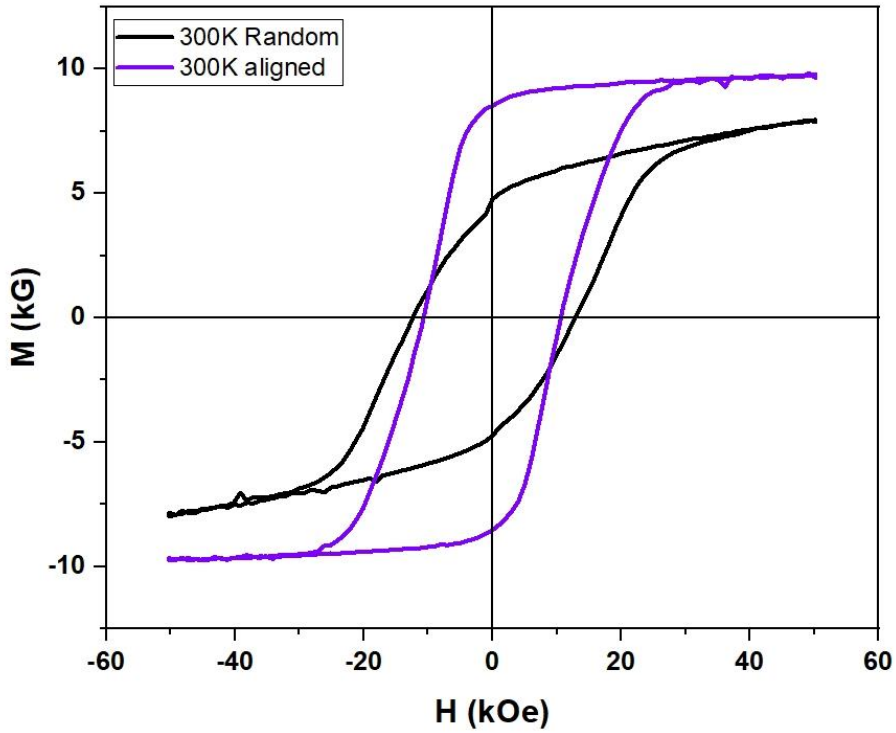

Figure 0-12. Hysteresis loop of as-printed (300K – Random) and post aligned (300K – aligned) AM-CM hybrid NdFeB/SmFeN PA12 magnet shows a decrease in remanence and increase in coercivity values compared to the AM only sample

1.13.5 Scanning electron microscopy (SEM) of hybrid NdFeB/SmFeN – bonded magnets

SEM was performed on as extruded cross section and tensile fracture surface of the small scale AM and AM-CM samples. In the as extruded sample, as seen in Figure 3-13, the smaller SmFeN particles adhere well to the binder but there is weak bonding to the NdFeB particles, likely due to lack of compaction. The fractography shows adhesive fracture closer to the center of the cross section whereas higher porosity is observed further away from the center indicating presence of higher defects in the surface or near-surface region.

In the small scale AM tensile fracture surface Figure 3-14 crack propagation is observed along the direction of print layer interfaces, suggesting weak interlayer bonding. Particle homogeneity across the sample volume is observed indicating high dispersion. The fracture surface is also non-withered across the sample with high porosity observed near the larger NdFeB particles. For the AM-CM tensile fracture surface Figure 3-15, a homogenous compound is observed with compact particle packing. Compared to the AM only fracture surface, a withered fracture surface with microcrack propagation at the interface of matrix and SmFeN particles is observed. Porosity is limited and with regions of microporosity present between the smaller SmFeN particles and matrix whereas larger NdFeB interfaces show a adhesive fracture, likely causing a brittle failure mode and high stiffness of the compound.

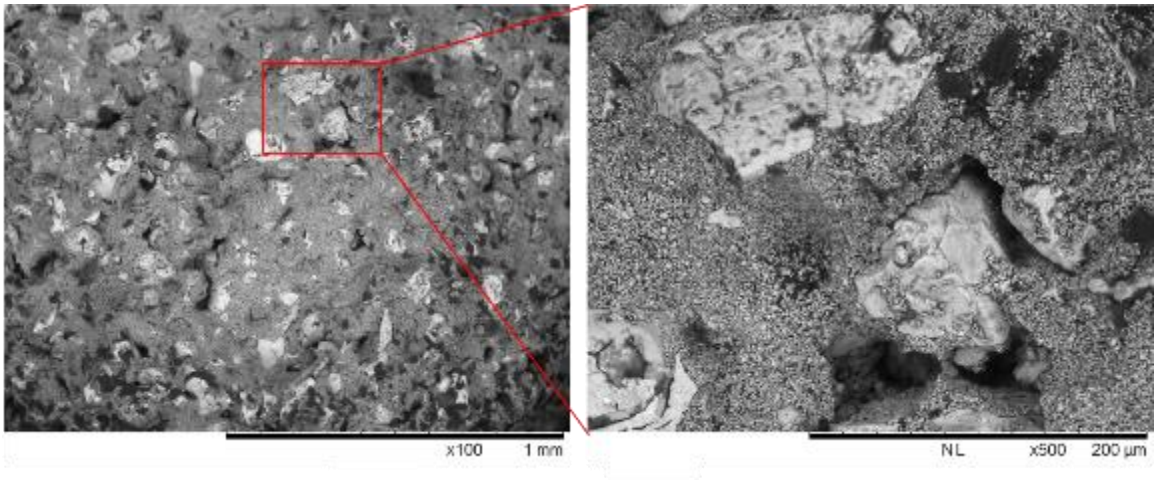

Figure 0-13. Scanning electron microscopy of the as extruded circular cross section shows higher porosity further the distance from center of cross section.

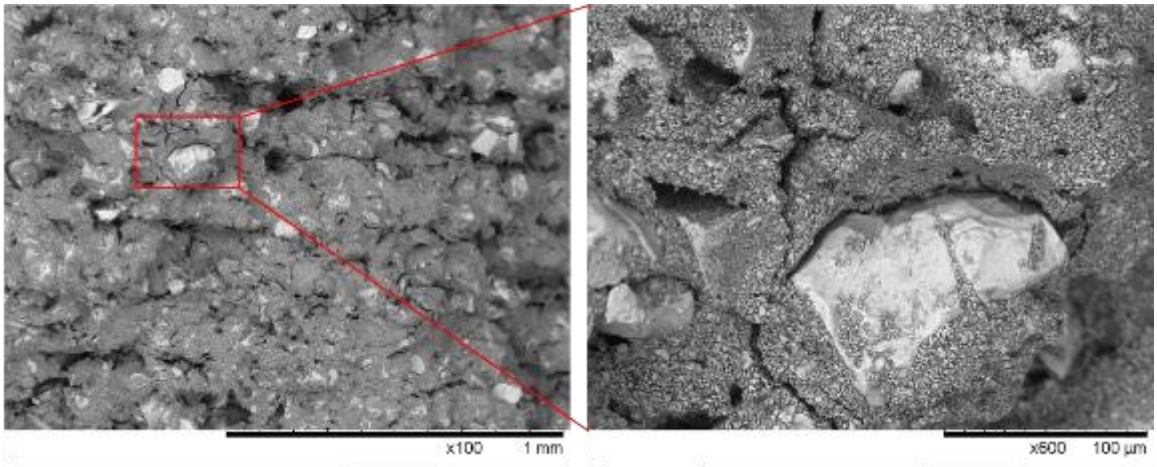

Figure 0-14. Scanning electron microscopy of the tensile fracture surface of small scale AM samples shows crack propagation along the layer interfaces and presence of porosity near the larger NdFeB particles

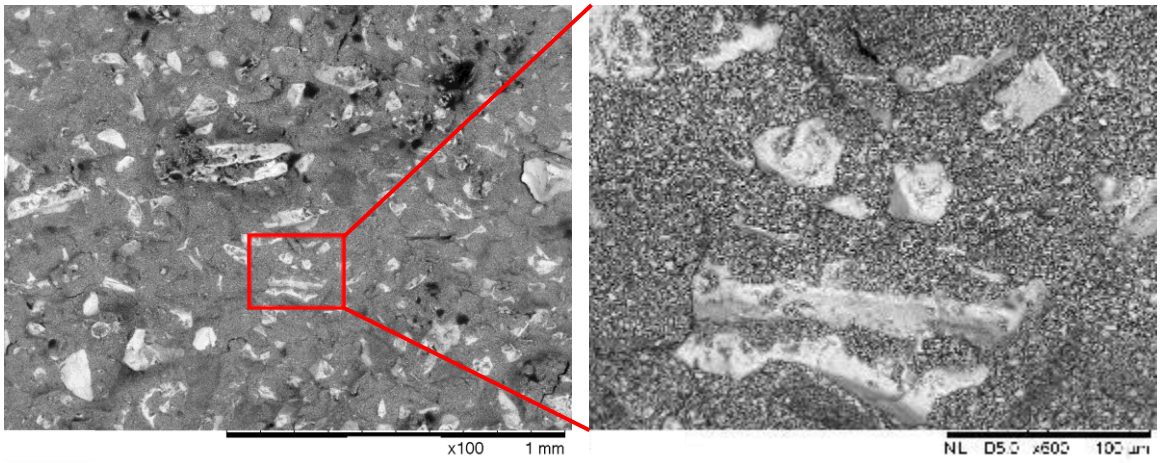

Figure 0-15. Scanning electron microscopy of the tensile fracture surface of AM-CM sample shows limited porosity, withered fracture surface and microcrack propagation at the SmFeN-matrix interface.

1.14 Conclusion

In this chapter, hybrid NdFeB-SmFeN bonded magnets in a PPS and PA12 matrix were studied. NdFeB-SmFeN/PPS magnets were densified by adding the larger NdFeB powder to the as received hybrid magnets and increasing the volume packing fraction during the compounding process followed by compression molding. It was found that significant increases in magnetic properties were obtained with Br of 10.4 kG, Hci of 10.8 kOe, and a (BH)max of 159 kJ/m^3. Density of the obtained magnet was 20 % higher than as received pellets at 6.15 g/cc. The NdFeB-SmFeN/PA12 magnets were studied using small scale additive manufacturing and large scale integrated additive manufacturing-compression molding with the objective of investigating alternate process to the traditional injection molding process. Parametric study and characterization were conducted and both small scale and large scale AM processes were at par with injection molding while being low cost. The mechanical and magnetic properties of the AM-CM magnet was equal or close to the industry reported injection molding data with tensile strength at 26 MPa, B_r of 8.5 kG, H_{ci} of 11.05 kOe, and a $(BH)_{max}$ of 117 kJ/m^3. Small scale AM showed slightly higher magnetic strength (6%) than AM-CM with 9.48 kG, H_{ci} of 10.65 kOe, BH_{max} of 124.14 kJ/m^3. However, the tensile strength was ~23% lower than AM-CM due to poor interlayer bonding and presence of porosity as shown by the fractography analysis conducted with SEM.

Chapter 4

1.15 Introduction

Chapter 4 investigates densification of samarium bonded magnets with a focus on magnetic field and temperature dependence on magnetic properties such as coercivity, remanence and maximum energy product. Also, application of compression bonded magnets in synchronous motors using overmolding is studied.

1.15.1 Samarium bonded magnets

Samarium iron nitride ($Sm_2Fe_{17}N_3$) magnets represent an important class of anisotropic magnets with high magnetic strength (BH_{max}~475 kJ/m^3), curie temperature (476 ºC) and uniaxial anisotropy (K_1=8.6).[44-46] SmFeN was developed after the breakthrough showing that insertion of interstitial atoms in ferromagnetic compounds can increase properties such as curie temperature and magnetocrystalline anisotropy.[60] Although SmFeN exhibits properties at par with Nd-Fe-B, it has processing challenges due to instability of the nitride at high temperatures.[11] The nitride decomposes at 600ºC, resulting in loss of magnetic properties, thus eliminating processes such as sintering as methods of production.[45] Liquid phase sintering is a stable method to process Nd-Fe-B, in fact it offers advantages such as formation of Nd-rich liquid phase which surrounds the Nd-Fe-B grains and increases oxidation resistance, leading to improved anisotropy fields.[61] To enable use of liquid phase sintering for samarium magnets, addition of various samarium based eutectic alloys (Al, Cu, Zn, Fe as metal binders) to the SmFeN compound have shown to have improved magnetic properties by lowering the processing temperature for the sintering process.[62]

SmFeN powders can be granulated to sizes in the range of 1-5 µm without loss of coercivity seen in NdFeB powders milled bellow 100 µm.[19, 49] SmFeN is advantageous when used as a bonded magnet, with high coercivity and corrosion resistant compared to NdFeB bonded magnets. Conventional manufacturing methods such as compression molding and injection molding as well as advanced methods like additive manufacturing can be used to produce bonded magnets.[1, 63-66] It is known that compression molding is an effective process to maximize material packing and density of bonded magnets. This study uses Nichia SmFeN/PA12 pellets of grade L16, which has spherical single crystal particles of 3 µm diameter and a corrosion resistant coating. A batch mixer is used to produce very high-density compounds with addition of samarium-aluminum alloy ($Sm_{70}Fe_{14}Al_{16}$) to the as received industry grade pellets. The compounds are compression molded into flat plates for testing. A Vibrating Sample Magnetometer (VSM) is used for post molding alignment and testing the magnetic properties. Excellent enhancement in energy product compared to the as received bonded pellets. Magnetic field dependence on degree of alignment and coercivity are investigated for the different weight fractions. The particle-particle interaction seems to limit alignment of particles and thus leading to a lower coercivity. The temperature dependence on maximum energy product, remanence and coercivity are also studied. The crystal structure is analyzed using X-Ray Diffraction.

1.15.2 Application of NdFeB/SmFeN bonded magnets for manufacturing of synchronous motors

Sintered and bonded permanent magnets made from $Nd_2Fe_{14}B$ (NdFeB) are

widely used materials in various industries, such as wind energy, automotive, aerospace, and consumer electronics, due to their highly desirable magnetic properties. The major applications for permanent magnets include electric motors, wind turbine generators, and computer hard disk drives (HDD).[67-69] With the energy product of bonded permanent magnets increasing over the past few years, their use in applications such as surface permanent magnet motors (SPM) and internal permanent magnet (IPM) is increasing. IPMs have a performance advantage over SPMs but require post-processing that includes machining and adhesive bonding of the magnet to the yoke/shaft.[70] The strength of the adhesive is also a limiting factor for the rotor mechanical strength. In this study, with use of thermoplastic bonded magnets and compression overmolding method, the potential to lower costs and enhance are demonstrated.[71] Commercial permanent magnets are generally manufactured by pressing and sintering magnetic powder. These magnets have high density and magnetic strength; however, they utilize critical materials such as neodymium (Nd), terbium (Tb), dysprosium (Dy) and other rare earth (lanthanide) elements, consequently making them expensive.[72] Conversely, hard ferrite magnets are low in magnetic strength but are relatively cheap to produce because they do not contain critical materials [7]. NdFeB are valued for high magnetic quality, while hard ferrites are valued for their low costs. In fact, the most sold hard magnets by monetary value are NdFeB, while the most sold by mass are hard ferrites. Due to the imported high price of manufactured NdFeB, there is a high demand for the conservation of NdFeB. One such conservation method is via manufacturing of bonded NdFeB. [63-66, 73, 74] Such magnets

comprise of a polymer binder in addition to the NdFeB powder. Sintered NdFeB are often made in simple shapes and need machining to reach the desired shape for the application, which may result in substantial wastage of rare earth material. With the use of formative manufacturing techniques such as injection molding and compression molding, bonded magnets can be made into shapes of much higher shape complexity without material wastage. This research builds upon previous study as shown in Chapter 2, 3.1 of compression molding of NdFeB and combines aspects of premixing and compression molding to fabricate NdFeB/SmFeN geometrically complex magnets and high material loading, density, and magnetic strength. SmFeN was chosen due to its excellent magnetic properties such as high Curie temperature (750 K), saturation magnetization (1.54-1.57 T), as well as its ability to be rendered into small particles without affecting said magnetic properties. The smaller SmFeN particles (3 μm) can be mixed into the interstitial spacing between the much larger NdFeB particles (100 μm), allowing a bi-modal mixing that results in higher packing densities and overall magnetic properties.

1.16 Materials and methods

1.16.1 Compression molding of samarium bonded magnets

Composite pellets of compounded Sm-Fe-N (Nichia Corporation) in nylon PA12 were mixed with samarium-aluminum alloy ($Sm_{70}Fe_{14}Al_{16}$) and compounded using batch mixing followed by compression molding. The details of the process are reported in previous chapters. (Chapter 2, 3.1) The magnetic hysteresis loops of both as printed and post aligned bonded magnets along the easy axis (parallel) were measured at 300K- 400 K

using a Quantum Design SQUID magnetometer. X-ray diffraction of as printed bonded magnets was performed with a Bruker diffractometer using Cu-Ka radiation.

SmFeN bonded magnets were printed with three different wt% of magnetic powder loading i.e. 92, 95 and 97 wt% is denoted as S1, S2 and S3 respectively. The batch mixed compound did not require a significant residence time in the batch mixer to form a homogeneous mixture. Lower residence time indicates less specific energy requirements in regard to mixing, and thus makes scaling up to large scale processes easier. Magnetic hysteresis loops at 300 K of the as-made bonded magnets were measured for each sample prior to in situ alignment in the SQUID magnetometer. Samples were then heated in a magnetic field, H_i, from 300 K to 512K temperature soaked for 5 minutes with magnetic field still being applied, and then cooled to 300 K, where magnetic hysteresis loops were measured again. For each alignment magnetic field strength, samples were heated to alignment temperatures, T = 513K at 12 degrees/min. Low to high temperature measurements was carried out from 20K to 400K, hysteresis loop were measured at each targeted temperature.

1.16.2 Compression overmolding of hybrid neodymium samarium magnets

Composites magnets comprised of Magfine anisotropic (Aichi Steel) NdFeB and SmFeN hybrid powder, henceforth MF15, and polyphenylene sulfide, henceforth PPS. A polymer batch mixer (Brabender Plasicordere W50) was used for hot melt processing of the MF15/PPS compounds. The batch mixer was used to produce a mixture of 93 weight percent of MF15 magnet powders with 7 weight percent PPS. This mixture is extruded and

then pelletized. These pellets were added to the batch mixer and an extruded charge was produced. Further information on how the batch mixer was operated has been described in previous work. The mold was preheated to 280˚C with an additively manufactured Fe3Si rotor part placed inside the cavity. Selective Laser Sintering process was used to manufacture the rotor part.[73] Figure 4-1(a,b) shows the SLS process during and after printing. The printed part is sliced using electric discharge machining (EDM), as shown in Figure 4-1(c). The extruded material was then compression molded at a pressure of 11.49 MPa with a dwell time of 20 min. A 30-ton hydraulic press (Carver, Model #3895) was used for the molding. The schematic of the over-molding process is shown in Figure 4-2. The charge was placed above the laser additively fabricated Fe3Si part and compressed into the holes for the rotor magnets. Excess charge/flash is removed after the compression molding via cutting and machining. Use of precise charge size or advanced manufacturing techniques such as additive manufacturing can minimize any post processing requirements.

The molded rotors were then cut into quarter sections via water jet cutting and mounted in epoxy for mechanical testing. Nanohardness indentation on the steel rotor and compression molded magnets were measured to understand the strength of the molded part. The testing was performed on a TI 950 TriboIndenter (Hysitron Incorporated). Additional macro-level strength evaluation was performed by measuring Vickers hardness using a Wilson VH1202 microhardness tester (Buehler, Lake Bluff, Illinois) with a load of 0.5 kg and a dwell time of 10 sec. The magnetic properties of both compounded and compressed

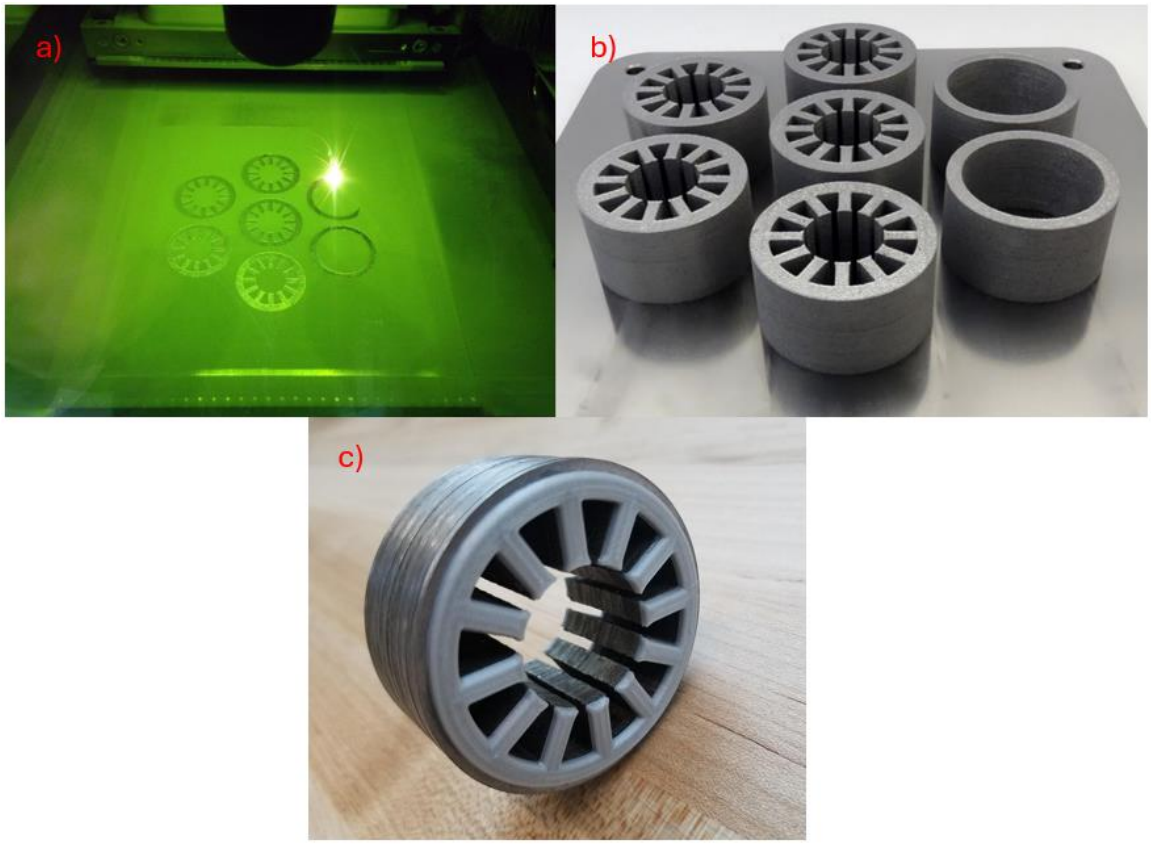

Figure 0-1 (a) Selective Laser Sintering (SLS) of Fe3Si rotor part; (b) Completed print; (c) Stacked slices of rotor parts after electrical discharge machining (EDM) shows the process flow used to manufacture the insert for overmolding. [73]

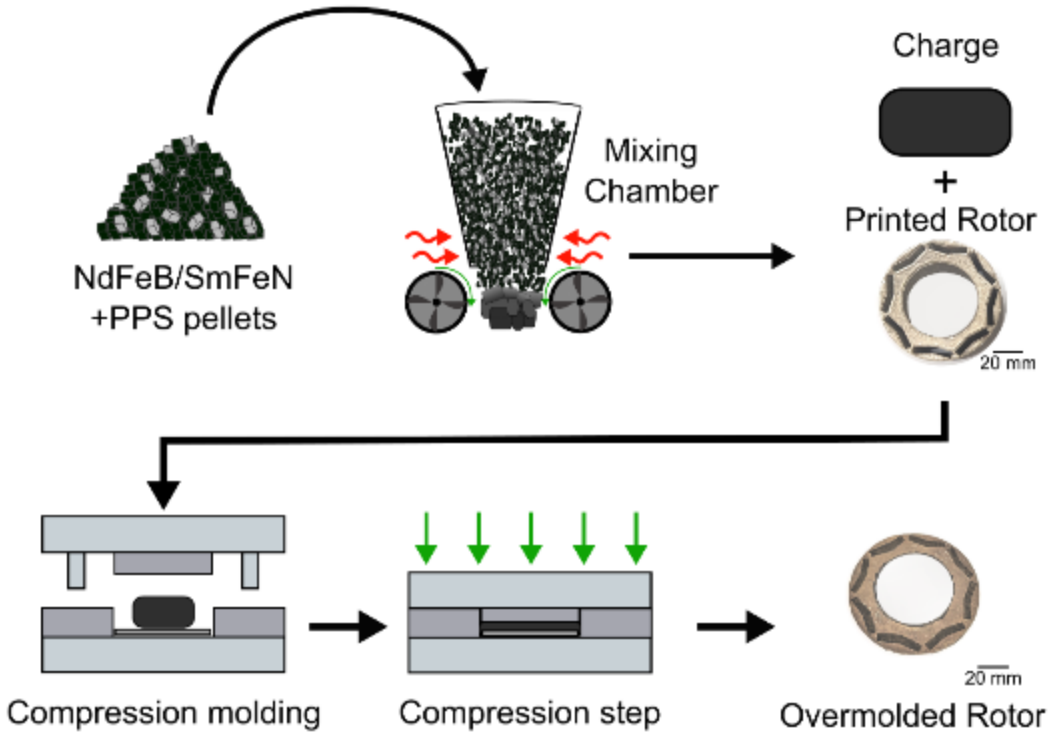

Figure 0-2 Schematic flow-chart of heating as-received composite magnetic pellets to final insert/over-molding of the printed Fe-3Si rotor. The charge is placed on top of the insert in a preheated mold before compression molding.

bonded magnet portion were measured using a Quantum Design SQUID magnetometer on the as-compressed bonded magnet and after an application of a 2T aligning field and annealing up to 625 K in 2T magnetic field. The as-compounded sample's field dependent magnetization at 300 K was measured and energy products were determined. Optical micrographs were taken with a VHX-5000 digital microscope (Keyence Corporation of America). Scanning electron microscopy (SEM) images were taken on a Merlin FE-SEM (Zeiss Group).

The magnetic properties of both compounded and compressed bonded magnet portion were measured using a Quantum Design SQUID magnetometer on the as-compressed bonded magnet and after an application of a 2T aligning field and annealing up to 625 K in 2T magnetic field. The as-compounded sample's field dependent magnetization at 300 K was measured and energy products were determined. Optical micrographs were taken with a VHX-5000 digital microscope (Keyence Corporation of America). Scanning electron microscopy (SEM) images were taken on a Merlin FE-SEM (Zeiss Group).

1.17 Results and discussion

1.17.1 X-Ray Diffraction of samarium bonded magnets

The structural analysis of the additively printed Sm-Fe-N bonded magnets in PA12 was examined by XRD. Figure 4-3 shows the XRD pattern of the as-molded bonded magnet. The XRD studies indicate that Sm-Fe-N bonded magnets did not reveal multiphase undesired nitrides such as SmN, a-Fe and oxide phase, unlike other 3D metal printing

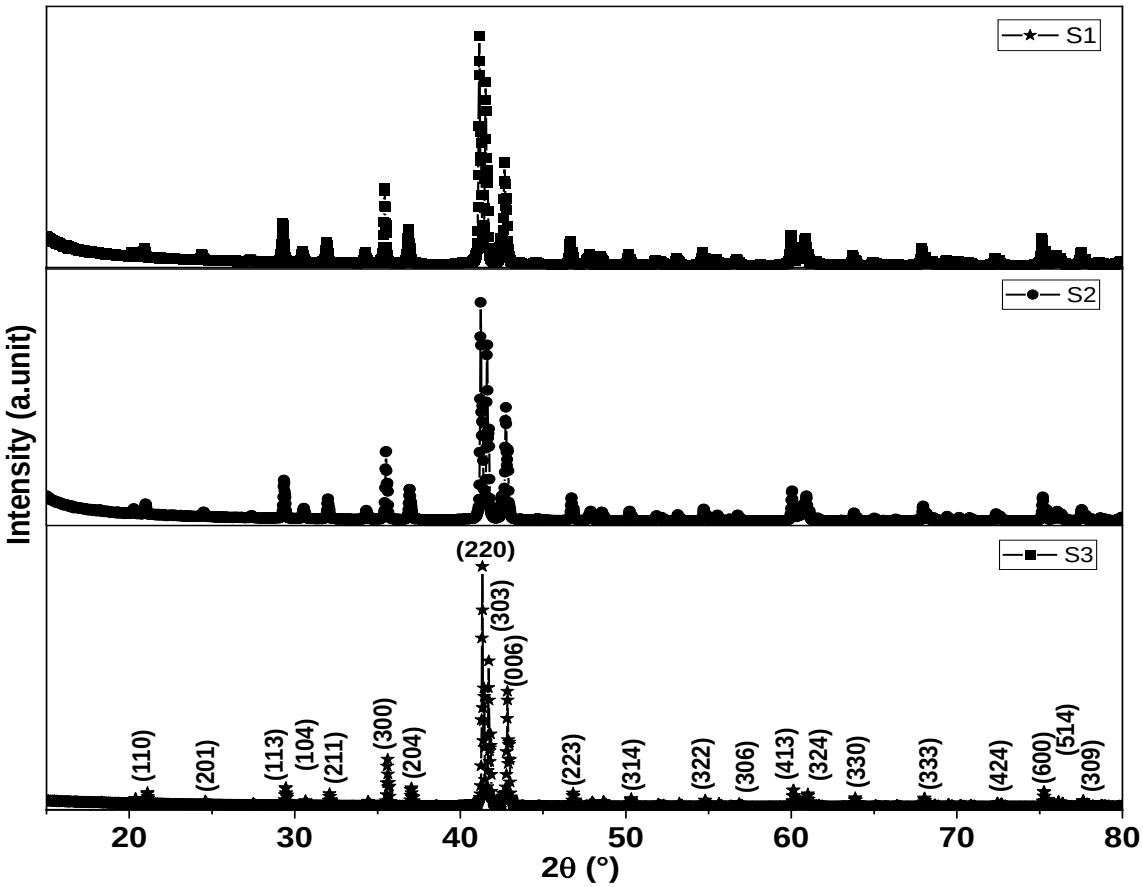

Figure 0-3. XRD of as-printed bonded magnets: Sm-Fe-N powder in PA12 matrix studies indicate that Sm-Fe-N bonded magnets did not reveal multiphase undesired nitrides such as SmN, a-Fe and oxide phase

techniques [75, 76] but only preserved the main $Sm_2Fe_{17}N_3$ phase. Hence, it can be concluded that the manufacturing process did not cause any degradation of the main phase of the initial magnetic powder.

1.17.2 Magnetic properties of samarium bonded magnets

1.17.2.1 Degree of Alignment dependence on weight fraction of compound

Figure 4-4 shows the magnetic hysteresis loops of compression molded Sm-Fe-N/PA12 bonded magnets before and after alignment. Three magnetic weight fractions of 92% (S1) , 95% (S2) and 97% (S3) are tested. Densities of S1, S2 and S3 are 4.6, 5.2 and 5.3gm/cm^3 respectively. It is observed that as the loading fraction of particles increases the coercivity decreases from 15.9 kOe, 13.4 kOe to 11.5 kOe for S1, S2 and S3 respectively. Saturation and remanence magnetization follow the same trend. Similar change in coercivity was studied O. Akdogan et all in SmCo5 particles interaction in C matrix. Sample S2 has attained the highest remanence magnetization 152 emu/g while S1 and S3 has remanence 148 and 146 emu/g respectively. To compare the effect of alignment at different fields, the degree of alignment (DoA) metric is used, defined as the remanence-to-saturation magnetization ratio (M_r/M_s). In Figure 4-5, DoA is seen to increase with alignment magnetic field and reaches its maximum value with applied magnetic field of H = 50 kOe for all three samples. However, the rate of alignment from 0-10kOe is slower for sample S3 than sample S1 and S2. During alignment, three types of material interactions are known to be present 1) Interaction between binder polymer and particles, 2) the interaction between applied magnetic field and particles 3) Particle - Particle interaction.

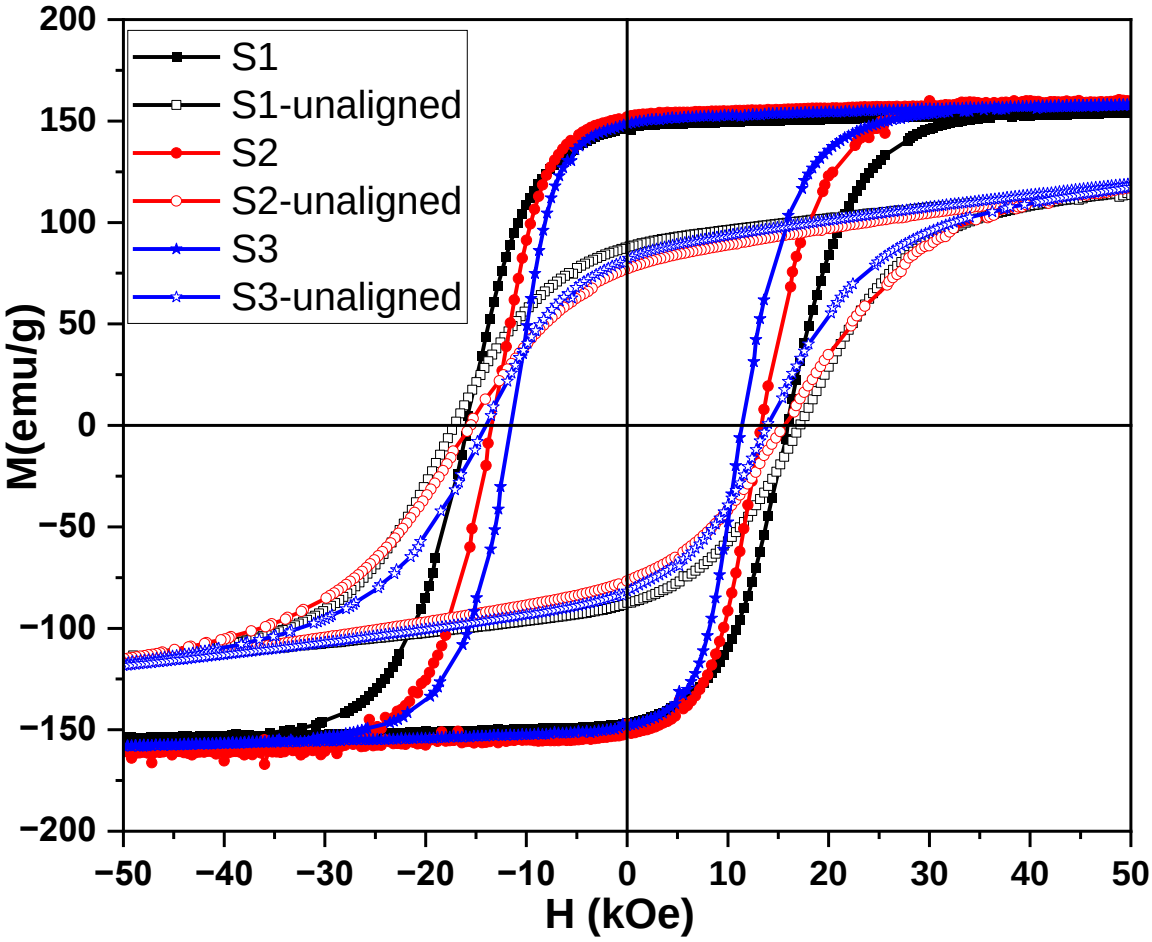

Figure 0-4. Magnetic hysteresis loops of SmFeN bonded magnets with various weight fractions: 92% (S1) , 95% (S2) and 97% (S3). S2 has the highest remanence value as well as a degree of alignment of 99%

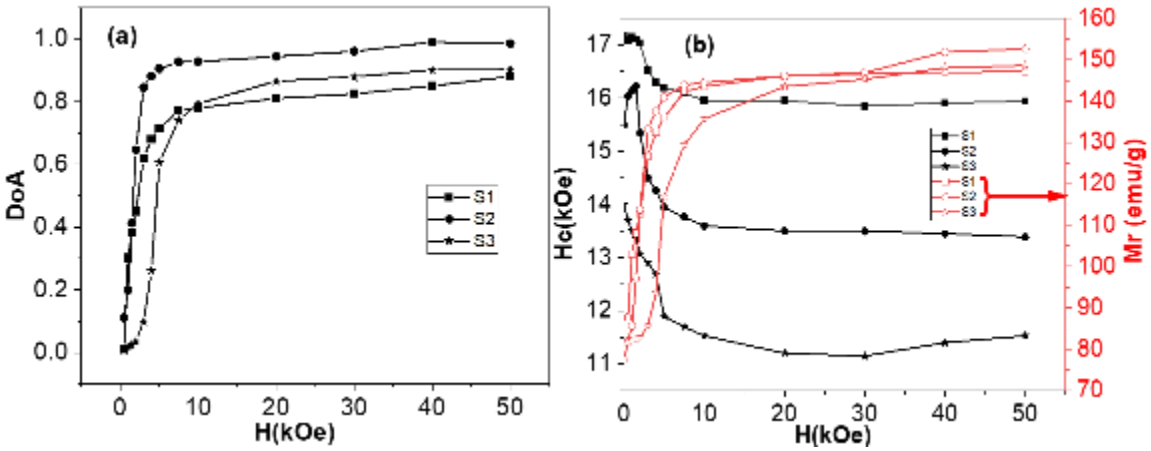

Figure 0-5. (a) Magnetic field dependent Degree of Alignment (DoA) for samples S1, S2 and S3 show a high rate of alignment of S2 sample (b) Change in coercivity(H_c) and remanence(M_r) during the alignment at different applied magnetic field for S2, S2 and S3 show S2 achieving highest remanence

This slow rate of alignment in sample S3 can be attributed to the dominance of particle-particle interaction due to a very high loading fraction. The maximum alignment 99% is achieved in S2, while S1 and S3 have 88% and 90% alignment. Thus, the weight fraction of 95% is determined to be optimal to achieve the highest DoA. Several factors can affect coercivity of the bonded magnets namely the increase in dipole interaction due to high magnetic fraction content, and the variation in the degree of grain alignment leading to plausible cause for the reduction in coercivity. [35, 77] Maximum energy product of 22.4 MGOe is achieved for S2 after alignment at 50kOe (Table 4-1).

1.17.2.1 Temperature dependent magnetic properties

The irreversible losses of the printed magnets were characterized with temperature coefficients of remanence *Br*, as α (%/K), and coercivity *Hc*, as β (%/K), using the second quadrant demagnetization characteristics obtained between 300 and 400 K, the change in coercivity and remanence is showed in Fig. 4-6 (a). The values show that the S1 has better thermal stability than S2 and S3. The better thermostability is explained by the low interparticle interaction. Fig. 4-6 (b) present the temperature dependent change in energy products, showing linear decrease in maximum energy product with increase in temperature, as expected. The second quadrant of S2 at low cryogenic temperature of 20k with incremental increases until room temperature (300K). It is evident that this sample is very stable even at 20K, and does not shows any spin re-orientation

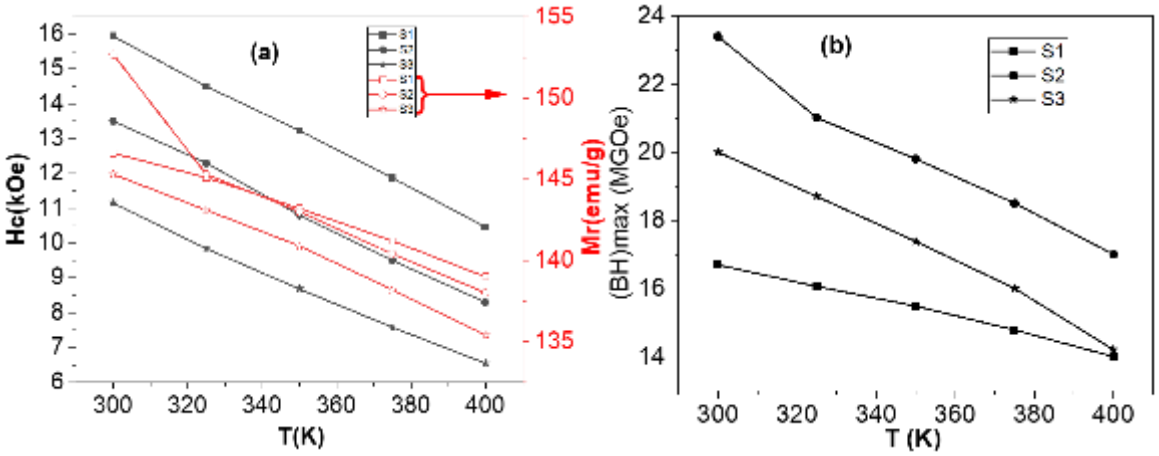

Figure 0-6. (a) Temperature dependent coercivity (H_c) and remanence (M_r) from 300K to 400K in 20K interval for S1, S2 and S3. (b) Temperature dependent energy product of S1, S2 and S3.

Table 0-1 Loading fraction wt%, Density, Energy product (BH)max, Degree of alignment (DoA) and thermal coefficient Alpha and Beta for S1, S2 and S3.

Sample	Mag powder weight fraction (%)	Density (g/cm^3)	(BH)max MGOe, 300K	DoA %	Thermal constant Alpha	Thermal constant Beta
S1	92	4.6	16.7	88	-0.34	-0.052
S2	95	5.3	23.4	99	-0.41	-0.068
S3	97	5.2	20.8	90	-0.41	-0.068

characteristic at low temperature. Hence, this magnet can successfully be used for low temperature applications as well.

1.17.3 Vickers and Nano- Hardness of overmolded hybrid magnets

The compression molded rotor was measured in both nano- and Vickers Hardness. Optical and SEM micrographs of both the in-planar and cross-sectional views are shown in Figures 4-7 and 4-8, respectively. Macro-scale strength measurements were performed on both in-planar and cross-sectional regions in the MF15/PPS overmolded Fe-3Si steel rotor to understand the difference in strength across the multi-material sample. 5 total measurements were taken from steel to polymer taken of each region and the average values and respective standard deviations are shown in Table 4-2.

For the in-planar view, the MF15/PPS has a larger average hardness than that of the Fe-3Si steel rotor (1.61 vs. 1.32 GPa) and is unexpected for these samples. However, the standard deviations for both regions on the in-planar view show high variance in the MF15/PPS region over the steel rotor. This behavior is attributed to the differences in size of the NdFeB and SmFeN particles in the polymer matrix. Large particles in this view would have greatly affected the overall average as pure NdFeB is reported to have a Vickers hardness between 0.7-0.9 GPa.[78, 79] The cross-sectional region has more expected values, where the MF15/PPS (0.75 ± 0.15 GPa) is lower in value than the steel rotor (1.85 ± 0.03 GPa). The discrepancy in the average values between the in-planar and cross-sectional views of the MF15/PPS region is most likely due to the particle alignment when compressed. The

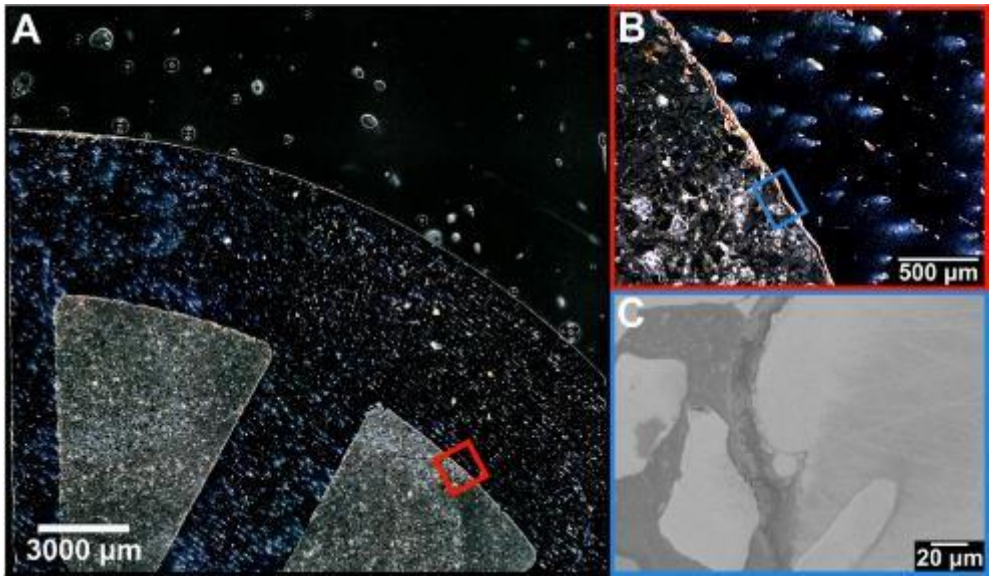

Figure 0-7. A) optical image of in-planar view of insert/over-molded rotor, B) higher magnification optical image of red square region shown in (A), and C) SEM image of blue region shown in (B). The red and blue colored borders indicates where the image with the colored border is located in the image not bordered by said color

Table 0-2. Vickers hardness indentation of overmolded MF15/PPS bonded magnets

Sample	Hardness (GPa)	Hardness (HV)
In plane (MF15/PPS)	1.61 ± 1.09	163.7 ± 112
In plane (AM Fe3Si steel rotor)	1.32 ± 0.14	134.1 ± 14.2
Cross sectional (MF15/PPS)	0.75 ± 0.15	76.0 ± 14.8
Cross sectional (Fe3Si) steel rotor	1.85 ± 0.03	189.1 ± 2.87

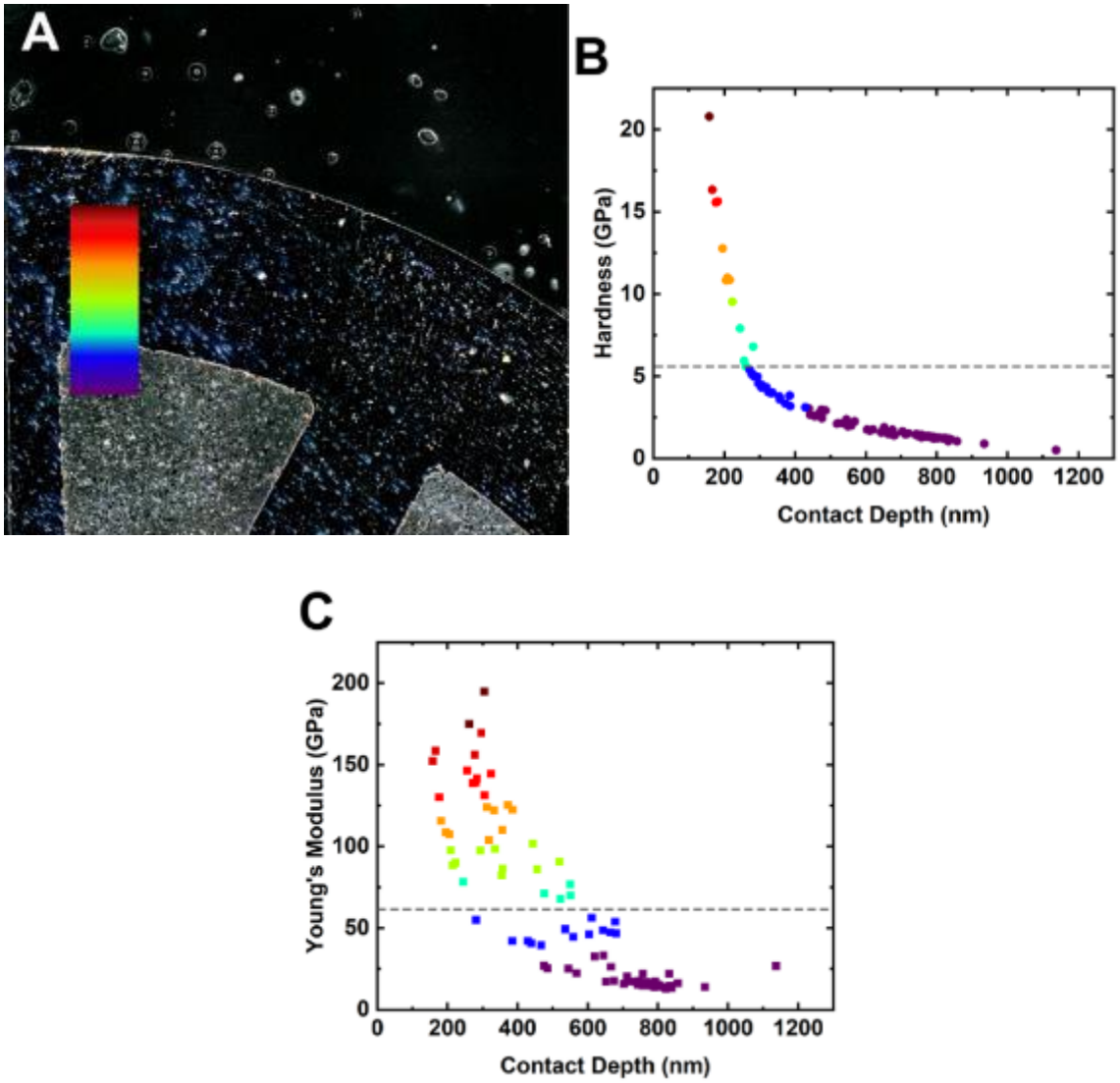

Figure 0-8. (A) The rotor and compression molded MF15/PPS with a color bar representing the hardness measurements. (B) Nano hardness vs. contact depth(C) Young's Modulus vs. contact depth.

compression molding step most likely caused preferential alignment of NdFeB and SmFeN particles along the plane of the printed steel rotor. Nano-hardness measurements were also taken on the in-planar sample to see the transition in strength from MF15/PPS to steel rotor. An overall image, hardness measurements, and strength data are shown in Figure 4-8. A gray dashed line is shown in both Figures 4-8(b) and 4-8(c) and it represents the transition from steel rotor to MF15/PPS. An additional color gradient is added to Figure 4-8(a) to graphically depict this transition. The steel rotor has harnesses and moduli that range from 5-20 GPa and 55-200 GPa respectively and are represented by dark red to cyan. The MF15/PPS section that was tested has harnesses below 5 GPa, young's modulus below 55 GPa and are represented by blues and purples. The discrete nature of the transition measurements from steel to polymer is a good sign that the union metal-matrix interface is strong and not affected by any defects due to the compression molding process. The strong interface is likely due to the fact that the Fe3Si rotor was machined using EDM after printing, offering a rough texture ideal for a strong mechanical bond as shown by previous studies. [80]

1.17.4 Magnetic properties of overmolded hybrid magnets

Magnetic material characterization was performed on the bonded magnet portion of the compression molded sample. The results from such testing are presented via Figure 4-9. The bonded magnet sample was magnetically annealed in a 2T applied magnetic field. The temperature increased from 300 K, to a high of 625 K, and then cooled back to 300 K. At 625K the measured sample was heated above the polymer's softening temperature to allow

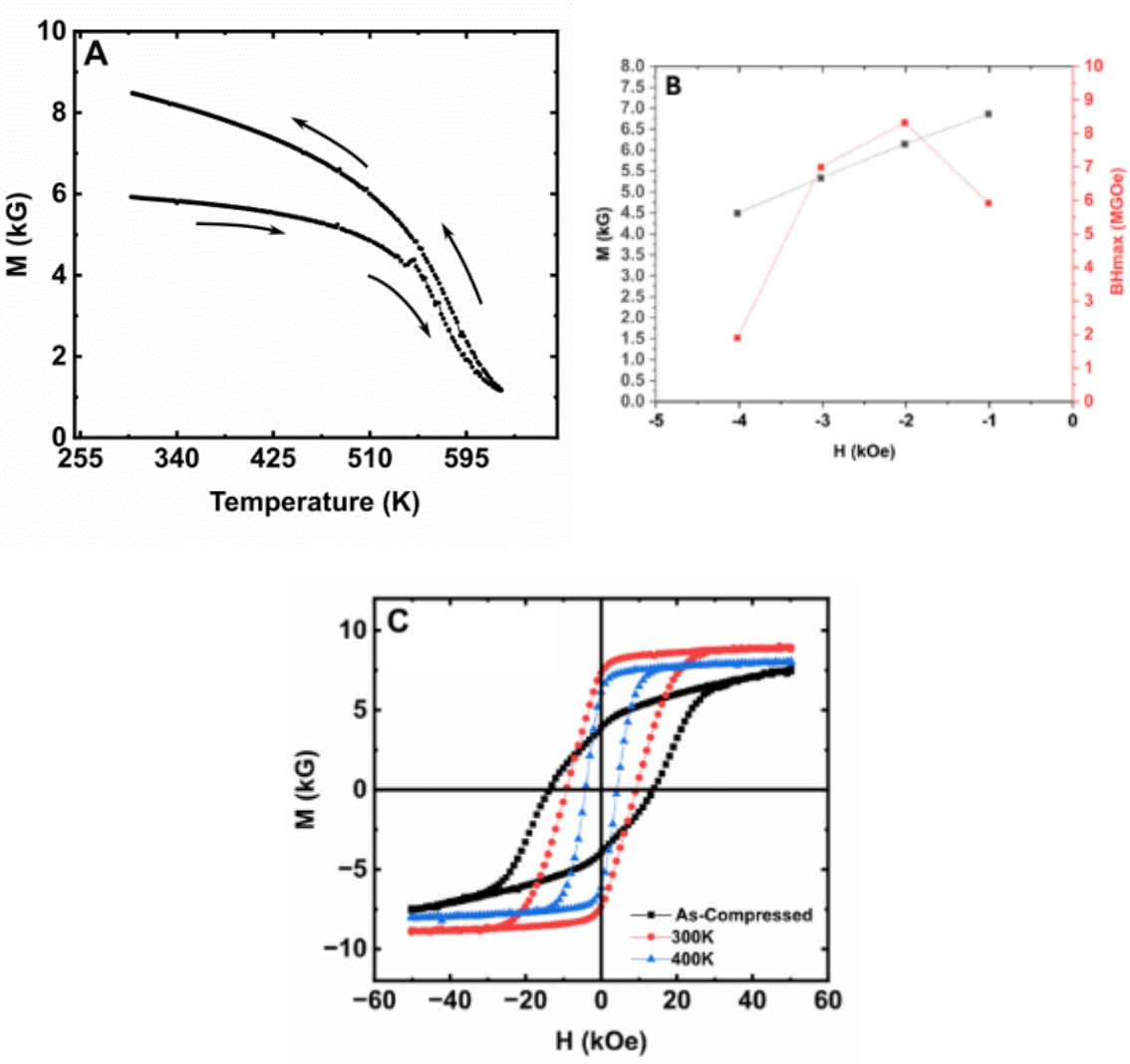

Figure 0-9. (A) M vs T plot (Magnetic alignment was done by annealing the sample from 300 to 625 K in a field of 2T and cooled back to 300K)- 625 K, (B) second quadrant magnetization and energy product of the magnetic material (measured at 300 K after annealing at 625K in 2T field and cooled down to 300 K), and (C) hysteresis loops measured as compressed, and at various temperatures (after post alignment at 625 K) 300 K and 400 K of the insert/over-molded bonded magnets

the magnetic particles to align in the direction of the applied magnetic field. Figure 4-9(a) shows the magnetization (M) of the sample as a function of temperature. Note that despite the start and end both being 300K, there is a significant increase in magnetization of the material after the full heat treatment of up to 625K and cooled back to 300K under magnetic field. Fig. 4.9(b) shows the 2nd quadrant of the hysteresis loop of the sample material. The magnetization and the energy product (BHmax) curves are shown. The measured coercivity of the sample is around 9 kOe, the remanence of the sample is approximately 7.3 kG, and the energy product of the sample is approximately 8.324 MGOe. Fig. 4.9(c) shows the hysteresis loops of the bonded magnet at various states. The black loop is the state of the sample as compressed. The red loop is the sample after magnetic alignment at 625 K in 2T field followed by cooling down to room temperature and measured at 300 K. The blue loop is after magnetic alignment at 625 K in 2T and cooled down to room temperature and measured at 400 K. 300 K produces the magnet with the highest saturation and remanent magnetization. At 400 K, lower magnetic properties are measured for the magnetic material. However, these properties are recovered when the material is brought back to lower temperatures, with the properties measured at 300 K post 400 K treatment the same as that measured at 300 K before 400 K treatment.

1.1 Conclusion

The research underscores the efficacy of compounding and compression molding techniques in enhancing the maximum energy product (BH_{max}) of Samarium Iron Nitride (SmFeN) bonded magnets within a PA12 matrix. Findings revealed that a weight fraction

of 95% yielded the highest BHmax of 186.21 kJ/m³ (23.4 MGOe), surpassing values of 132.89 kJ/m³ for 93% weight fraction and 165.52 kJ/m³ for 97% weight fraction magnets. Additionally, the degree of alignment (DoA) achieved 99% in the 95% weight fraction magnets, exceeding DoA values of 88% and 90% in the 93% and 97% weight fraction magnets, respectively. This superior alignment in the 95% weight fraction magnets is attributed to reduced particle-particle interaction during the post-manufacturing alignment process. Moreover, the 95% weight fraction samples exhibit greater strength compared to those with a 97% weight fraction. Furthermore, the research includes temperature-dependent magnetic property analysis, demonstrating the stability of the manufactured bonded magnets even at low temperatures down to 20K. The demonstrated stability across various temperature ranges underscores the potential applicability of these magnets across diverse industrial sectors, presenting opportunities for innovation and advancement in magnetic materials technology. Furthermore, MF15 (mixture of NdFeB and SmFeN) powders in a PPS matrix were compression molded into a 3D printed Fe-3Si steel rotor. Optical and SEM images show that the joint between the two materials is uniform and free of defects. Vickers and nano hardness were measured for both materials showing the steel rotor was harder in both cases. The magnetic properties of the small piece of the overmolded sample had a BH_{max} of 8.324 MGOe after post-magnetic field annealing. This work shows that higher performance magnets can be manufactured into existing components used in industry. Future work would need to investigate the feasibility of

processing the same magnetic material into larger scale steel components followed by post-magnetic field annealing for final use.

Chapter 5

1.2 Conclusion

In conclusion, this thesis conducted a comprehensive literature review and experimental investigation into bonded rare earth magnets, studying their synthesis, properties and potential applications. The study employed both conventional and advanced methodologies to fabricate and assess formulations of rare earth-based materials, with the aim of fulfilling the gap magnet strength requirements (100-150 kJ/m^3). Several key findings of the research are detailed below.

For the first objective of the research, the synthesis of bonded magnets was examined using techniques such as twin-screw extrusion, small scale batch mixing and compression molding. Anisotropic bonded NdFeB magnets [MQA grade] in a PC binder matrix are fabricated. Weight fraction of magnetic compounds was iteratively increased while simultaneously optimizing the process parameters. Extruder/mixer residence time, barrel temperatures, screw speed and material feed rate were identified as the key parameters playing a role in subsequent properties of the compound produced. To understand the role played by material composition, various weight fractions (w.f.) of NdFeB/PC on the batch mixer (20, 50, 75, 85 and 95%) are compared to the twin screw extruder with 20, 50 and 75% respectively. The density of the 95% (w.f.) batch mixed magnets fabricated was 5.34 g/cm3 and the magnetic properties were, intrinsic coercivity Hci = 942.99 kA/m, remanence Br = 0.86 T, and energy product (BH)max = 120.96 kJ/m3. The measured tensile properties are in the range of 27-59 MPa. Scanning electron microscopy was used to study the interface of the magnetic particles and the matrix. It was

concluded that compression molding technology plays a pivotal role in attaining maximum density of the compound while homogenous mixing and composition of the multi-material system contributed towards its mechanical strength.

Building upon the first objective, other rare earth iron based inter-metallics are studied. NdFeB/SmFeN hybrid material with a bimodal particle size distribution (PSD) are studied in the second objective of the research. Bimodal PSD allows efficient volumetric packing efficiency of the compound by packing the smaller SmFeN (3 μm particle size) within the space between the larger NdFeB (100 μm particle size) powders. Industry grade Magfine MF15P/PPS composite pellets were added with pure MF15P powder in the batch mixer to increase the weight fraction of the compound from 93% to 96%. The density of the 96% compound was 6.15 g/cm3 and maximum energy product (BHmax) was 159.16 kJ/m3. There is a slight reduction in the experimental remanence values by 3.5% compared to the theoretically attainable. The reduction may be related to imperfect magnetic alignment and the aim of future works is to bridge this gap using additive manufacturing followed by compression molding. The bimodal NdFeB/SmFeN-PA12 composite material was then processed on a pellet fed additive printer with a single screw extruder to produce compounds of 93% magnetic weight fraction. Manufacturing process variations in parameters such as layer height, nozzle size, nozzle temperature, screw speed and gantry feed rate are studied to obtain the highest possible density of the magnets. The density of the 93% wt. fr. printed magnets was 5.2 g/cm3 with a BH_{max} value of 124.14 kJ/m3. This

is a significant increase from the previous studies which utilized additive processes with the same loading fraction. [16, 34, 30]

Furthermore, having studied NdFeB and hybrid NdFeB/SmFeN bonded magnets, the third objective aimed to study SmFeN bonded magnets as well as. The study highlights the effectiveness of compounding and compression molding techniques in enhancing the maximum energy product (BH_{max}) of Samarium Iron Nitride (SmFeN) bonded magnets in a PA12 matrix. The investigation revealed that a weight fraction of 95% resulted in the highest maximum energy product (BH_{max}) of 186.21 kJ/m³ (23.4 MGOe) compared to 132.89 kJ/m^3 for 93 w.f. and 165.52 kJ/m³ for 97 w.f. magnets. Moreover, the degree of alignment (DoA) reached 99% in the 95 w.f. magnets, surpassing the 88% and 90% DoA achieved in the 93 and 97 w.f. magnets respectively. This superior alignment in the 95 w.f. magnets can be attributed to reduced particle-particle interaction during the post-manufacturing alignment process. In addition, 95 w.f. samples are much stronger than 97 w.f. samples. Additionally, the study conducted temperature-dependent magnetic property analysis, demonstrating the stability of the manufactured bonded magnets even at low temperatures down to 20K. The demonstrated stability across a range of temperatures further underscores the potential applicability of these magnets in various industrial sectors, offering opportunities for innovation and advancement in magnetic materials technology. Finally, to validate the potential of the above advanced manufacturing techniques, application development is conducted in the manufacturing of stator/rotor systems. In the preliminary product development work, a

blend of NdFeB/SmFeN hybrid powders in a polyphenylene sulfide (PPS) matrix is overmolded on a 3D printed iron silicon rotor insert using compression molding. Vickers and nano-hardness is measured of both the polymer blend and steel rotor. The magnet has a measured energy product of 8.3 MGOe. The demonstrated method provides a pathway for making high performance additively printed electric motors and generators.

1.3 Future research directions

Future research directions for further advancement in the field of bonded magnets could encompass several key areas:

Enhancement of Alignment Techniques: Develop innovative alignment techniques to achieve even higher degrees of particle alignment in bonded magnets. This could involve exploring magnetic field-assisted alignment methods or surface treatment techniques to minimize particle-particle interactions and optimize magnetic properties. Optimized study of process parameters for use in additive manufacturing done in Chapter 3 paves way to develop in-situ particle alignment techniques while printing the magnet, eliminating the need for post-alignment of the material.

Complete integration into other specific applications: Focus on integrating bonded magnets into applications such as, sensors, and actuators, to assess their performance in real-world scenarios.

Exploration of Sustainable Manufacturing Practices: Investigate environmentally friendly manufacturing practices for bonded magnets, including the use of recycled materials and alternative binders with lower environmental impact.

Sustainable manufacturing processes will be essential for reducing the environmental footprint of magnet production.

Multifunctional Magnet Development: Explore the possibility of developing bonded magnets with multifunctional properties, such as magnetocaloric or magnetostrictive effects, in addition to traditional magnetic properties. This could open up new avenues for applications in energy conversion, sensing, and actuation.

By addressing these future research directions, the field of bonded magnets can continue to evolve, leading to the development of advanced materials with enhanced performance and broader applicability across various industries.

References

1. Ormerod, J. and S. Constantinides, *Bonded permanent magnets: Current status and future opportunities.* Journal of Applied Physics, 1997. **81**(8): p. 4816-4820.
2. Chu, S., *Critical materials strategy*. 2011: DIANE publishing.
3. Commission, E., et al., *Methodology for establishing the EU list of critical raw materials – Guidelines*. 2017: Publications Office.
4. Keilhacker, M.L. and S. Minner, *Supply chain risk management for critical commodities: A system dynamics model for the case of the rare earth elements.* Resources, Conservation and Recycling, 2017. **125**: p. 349-362.
5. USDOE, *Critical Materials Rare Earths Supply Chain: A Situational White Paper*, o. Energy, Editor. 2020.
6. Lucas, J., et al., *Rare earths: science, technology, production and use*. 2014: Elsevier.
7. Sagawa, M., et al., *New material for permanent magnets on a base of Nd and Fe.* Journal of Applied Physics, 1984. **55**(6): p. 2083-2087.
8. Herbst, J. and J. Croat, *Neodymium-iron-boron permanent magnets.* Journal of magnetism and magnetic materials, 1991. **100**(1-3): p. 57-78.
9. *Manufacture of Modern Permanent Magnet Materials*. Available from: https://www.arnoldmagnetics.com/wp-content/uploads/2017/10/Manufacture-of-Modern-Permanent-Magnet-Materials-Constantinides-PowderMet-2014-ppr.pdf.
10. Kaneko, Y., et al., *Proven technologies on high-performance Nd–Fe–B sintered magnets.* 2006. **408**: p. 1344-1349.
11. Coey, J., *Perspective and prospects for rare earth permanent magnets.* Engineering, 2020. **6**(2): p. 119-131.
12. Sarriegui, G., et al., *Development of anisotropic Nd-Fe-B powder from isotropic gas atomized powder.* Powder Technology, 2024. **431**: p. 119067.
13. Ma, B., et al., *Recent development in bonded NdFeB magnets.* Journal of Magnetism and Magnetic Materials, 2002. **239**(1-3): p. 418-423.
14. Chikazumi, S. and C.D. Graham, *Physics of Ferromagnetism 2e*. 2009: Oxford University Press on Demand.
15. Miyazaki, T. and H. Jin, *The physics of ferromagnetism*. Vol. 158. 2012: Springer Science & Business Media.
16. Coey, J.J.S.S.C., *Permanent magnetism.* 1997. **102**(2-3): p. 101-105.
17. Zhou, S. and Q. Dong, *Super Permanent magnets—Permanent Magnetic Material of Rare-earth and Iron System*. 2004, Metallurgy Industry Publishing, Beijing.
18. Li, J., et al., *Effect of process on the magnetic properties of bonded NdFeB magnet.* 2006. **299**(1): p. 195-204.
19. Brown, D., B.-M. Ma, and Z. Chen, *Developments in the processing and properties of NdFeb-type permanent magnets.* Journal of magnetism and magnetic materials, 2002. **248**(3): p. 432-440.
20. Coey, J., *Permanent magnets: Plugging the gap.* Scripta Materialia, 2012. **67**(6): p. 524-529.

21. Brown, D., B.-M. Ma, and Z. Chen, *Developments in the processing and properties of NdFeb-type permanent magnets.* % Journal of magnetism magnetic materials, 2002. **248**(3): p. 432-440.
22. Nlebedim, I., et al., *Studies on in situ magnetic alignment of bonded anisotropic Nd-Fe-B alloy powders.* Journal of Magnetism and Magnetic Materials, 2017. **422**: p. 168-173.
23. Sheridan, R., et al., *Improved HDDR processing route for production of anisotropic powder from sintered NdFeB type magnets.* 2014. **350**: p. 114-118.
24. Sugimoto, S., et al., *Resistivity measurements on hydrogenation disproportionation desorption recombination phenomena in Nd Fe B alloys with Co, Ga and Zr additions.* 1997. **260**(1-2): p. 284-291.
25. Magnaquench. *https://mqitechnology.com/products/bonded-neo-powder/*.
26. Magnaquench. *https://mqitechnology.com/wp-content/uploads/2017/09/mqfp-brochure.pdf*.
27. B.M. Ma, et al. *Proceedings of the 10th Conference on Magnetism and Magnetic Technology, 1995, p. 83.* 1995.
28. Pinkerton, F.E., et al., *Thermal aging of melt-spun NdFeB magnetic powder in hydrogen.* 2016. **417**: p. 106-111.
29. Li, D., et al., *Liquid coated melt-spun Nd–Fe–B powders for bonded magnets.* 1999. **85**(8): p. 4871-4873.
30. Gao, R., et al., *Dependence of the magnetic properties on the alignment magnetic field for NdFeB bonded magnets made from anisotropic HDDR powders.* 1999. **191**(1-2): p. 97-100.
31. Kronmüller, H., et al., *Angular dependence of the coercive field in sintered Fe77Nd15B8 magnets.* 1987. **69**(2): p. 149-157.
32. Li, L., et al., *Big area additive manufacturing of high performance bonded NdFeB magnets.* Scientific Reports, 2016. **6**: p. 36212.
33. Zhai, F., et al., *Epoxy resin effect on anisotropic Nd–Fe–B rubber-bonded magnets performance.* Journal of allloys and compounds, 2011. **509**(3): p. 687-690.
34. Liu, W., et al., *Preparation and characterization of sodium silicate/epoxy resin composite bonded Nd-Fe-B magnets with high performance.* 2019. **37**(10): p. 1083-1087.
35. Coey, J. and K.J.J.o.a.p. O'Donnell, *New bonded magnet materials.* 1997. **81**(8): p. 4810-4815.
36. Paranthaman, M.P., et al., *Binder jetting: A novel NdFeB bonded magnet fabrication process.* Journal of The Minerals, Metals & Materials Society, 2016. **68**(7): p. 1978-1982.
37. Gandha, K., et al., *Additive manufacturing of highly dense anisotropic Nd–Fe–B bonded magnets.* Scripta Materialia, 2020. **183**: p. 91-95.
38. Compton, B.G., et al., *Direct-write 3D printing of NdFeB bonded magnets.* Journal of Materials and Manufacturing Processes, 2018. **33**(1): p. 109-113.

39. Garrell, M.G., et al., *Mechanical properties of Nylon bonded Nd–Fe–B permanent magnets.* Journal of Magnetism and Magnetic Materials, 2003. **257**(1): p. 32-43.
40. Garrell, M.G., et al., *Mechanical properties of polyphenylene-sulfide (PPS) bonded Nd–Fe–B permanent magnets.* Journal of Material Science and Engineering: A, 2003. **359**(1-2): p. 375-383.
41. Dobrzański, L., et al., *Mechanical properties and the structure of magnetic composite materials.* Journal of Achievements in Materials and Manufacturing Engineering, 2006. **18**(1-2): p. 79-82.
42. Liu, J., et al., *Microstructure and magnetic properties of sintered NdFeB magnets with improved impact toughness.* Journal of Applied Physics, 2005. **97**(10): p. 10H101.
43. *Brabender Plasticorder technical design sheet*. Available from: https://webport.brabender.com/s9MqLziYXN.
44. Iriyama, T., et al., *Effect of nitrogen content on magnetic properties of Sm/sub 2/Fe/sub 17/N/sub x/(0< x< 6).* IEEE transactions on magnetics, 1992. **28**(5): p. 2326-2331.
45. Christodoulou, C.N. and N. Komada, *High coercivity anisotropic Sm2Fe17N3 powders.* Journal of alloys and compounds, 1995. **222**(1-2): p. 92-95.
46. Coey, J., et al., *Sm-Fe-N revisited; remanence enhancement in melt-spun Nitroquench material*. Journal of Magnetism and Magnetic Materials, 2019. **480**: p. 186-192.
47. Gandha, K., et al., *Additive manufacturing of anisotropic hybrid NdFeB-SmFeN nylon composite bonded magnets.* Journal of Magnetism and Magnetic Materials, 2018. **467**: p. 8-13.
48. Nothnagel, P., et al., *The influence of particle size on the coercivity of sintered NdFeB magnets.* Journal of magnetism and magnetic materials, 1991. **101**(1-3): p. 379-381.
49. Kurniawan, C., et al. *Effect of particle size distribution on the preparation of bonded NdFeB permanent magnet*. in *IOP Conference Series: Materials Science and Engineering*. 2019. IOP Publishing.
50. Ma, B., et al., *Preparation of anisotropic bonded NdFeB/SmFeN hybrid magnets by mixing two different size powders.* Journal of Magnetism and Magnetic Materials, 2018. **457**: p. 70-74.
51. Yamashita, F., et al., *Composite bonded magnets with controlled anisotropy directions prepared by viscous deformation technique.* Journal of Magnetism and Magnetic Materials, 2007. **316**(2): p. e101-e104.
52. Zheng, J., W.B. Carlson, and J.S. Reed, *The packing density of binary powder mixtures.* Journal of the European Ceramic Society, 1995. **15**(5): p. 479-483.
53. Brewe, J.E. and J.J. Myers, *Particle size optimization for reduced cement high strength concrete.* Proceedings of the PCI-NBC on Bridges for Life, 2005.
54. Gandha, K., et al., *Additive manufacturing of highly dense anisotropic Nd–Fe–B bonded magnets.* 2020. **183**: p. 91-95.

55. Coey, J. and H. Sun, *Improved magnetic properties by treatment of iron-based rare earth intermetallic compounds in anmonia.* Journal of Magnetism and magnetic materials, 1990. **87**(3): p. L251-L254.
56. Tymrak, B., M. Kreiger, and J.M. Pearce, *Mechanical properties of components fabricated with open-source 3-D printers under realistic environmental conditions.* Materials & Design, 2014. **58**: p. 242-246.
57. Letcher, T., B. Rankouhi, and S. Javadpour. *Experimental study of mechanical properties of additively manufactured ABS plastic as a function of layer parameters*. in *ASME international mechanical engineering congress and exposition*. 2015. American Society of Mechanical Engineers.
58. Doshi, M., et al., *Printing parameters and materials affecting mechanical properties of FDM-3D printed Parts: Perspective and prospects.* Materials Today: Proceedings, 2022. **50**: p. 2269-2275.
59. Giri, J., et al., *Effect of process parameters on mechanical properties of 3d printed samples using FDM process.* Materials Today: Proceedings, 2021. **47**: p. 5856-5861.
60. Otani, Y., et al., *Magnetic properties of a new family of ternary rare-earth iron nitrides R2Fe17N3− δ.* Journal of applied physics, 1991. **69**(8): p. 5584-5589.
61. Vial, F., et al., *Improvement of coercivity of sintered NdFeB permanent magnets by heat treatment*. Journal of magnetism and magnetic materials, 2002. **242**: p. 1329-1334.
62. Otogawa, K., K. Takagi, and T. Asahi, *Consolidation of Sm2Fe17N3 magnets with Sm-based eutectic alloy binder.* Journal of Alloys and Compounds, 2018. **746**: p. 19-26.
63. Gandha, K., et al., *Additive manufacturing of highly dense anisotropic Nd–Fe–B bonded magnets.* Scripta Materialia, 2020. **183**: p. 91-95.
64. Mungale, K., et al., *Compression molding of anisotropic NdFeB bonded magnets in a polycarbonate matrix.* Materialia, 2021. **19**: p. 101167.
65. Domingo-Roca, R., J. Jackson, and J. Windmill, *3D-printing polymer-based permanent magnets.* Materials & Design, 2018. **153**: p. 120-128.
66. Li, L., et al., *Big area additive manufacturing of high performance bonded NdFeB magnets.* Scientific reports, 2016. **6**(1): p. 1-7.
67. Coey, J., *Permanent magnet applications.* Journal of Magnetism and Magnetic Materials, 2002. **248**(3): p. 441-456.
68. Farina, A. and A. Anctil, *Material consumption and environmental impact of wind turbines in the USA and globally.* Resources, Conservation and Recycling, 2022. **176**: p. 105938.
69. Ueberschaar, M. and V.S. Rotter, *Enabling the recycling of rare earth elements through product design and trend analyses of hard disk drives.* Journal of Material Cycles and Waste Management, 2015. **17**: p. 266-281.

70. Jha, A.K., et al. *Design and comparison of outer rotor bonded magnets Halbach motor with different topologies*. in *2017 15th International Conference on Electrical Machines, Drives and Power Systems (ELMA)*. 2017. IEEE.
71. Zubkov, Y., Y. Makarichev, and M. Alimbekov. *How Permanent Magnets Bonding Methods Affect the Rotor Mechanical Strength in an SPM Synchronous Starter*. in *2019 International Conference on Industrial Engineering, Applications and Manufacturing (ICIEAM)*. 2019. IEEE.
72. Hirosawa, S., *Current status of research and development toward permanent magnets free from critical elements.* Journal of the Magnetics Society of Japan, 2015. **39**(3): p. 85-95.
73. Lamichhane, T.N., et al., *Additively manufactured Fe-3Si stator for a high-performance electrical motor.* Available at SSRN 4525351, 2022.
74. Paranthaman, M.P., et al., *Binder jetting: A novel NdFeB bonded magnet fabrication process.* Jom, 2016. **68**: p. 1978-1982.
75. Jacimovic, J., et al., *Net shape 3D printed NdFeB permanent magnet.* arXiv preprint arXiv:1611.05332, 2016.
76. Metelkova, J., et al., *Improving the quality of up-facing inclined surfaces in laser powder bed fusion of metals using a dual laser setup.* Procedia CIRP, 2020. **94**: p. 266-269.
77. Gao, R., et al., *Dependence of the magnetic properties on the alignment magnetic field for NdFeB bonded magnets made from anisotropic HDDR powders.* Journal of magnetism and magnetic materials, 1999. **191**(1-2): p. 97-100.
78. Gao, Y., et al., *Corrosion resistance, mechanical and magnetic properties of cold-sprayed al coating on sintered NdFeB magnet.* Journal of Thermal Spray Technology, 2021. **30**(8): p. 2117-2127.
79. Wang, G., et al., *Effects of sintering temperature on the mechanical properties of sintered NdFeB permanent magnets prepared by spark plasma sintering.* Journal of magnetism and magnetic materials, 2014. **349**: p. 1-4.
80. Novák, L., et al., *Surface modification of metallic inserts for enhancing adhesion at the metal–polymer interface.* Polymers, 2021. **13**(22): p. 4015.

Vita

Kaustubh Mungale was born in Navi Mumbai, India on December 4th, 1994. He earned his bachelor's degree in 2016 with a Mechanical Engineering major. Upon completion of his undergraduate studies, Kaustubh moved to the United States to pursue a master's degree in 2017 at the University of Tennessee, Knoxville and changed his program to pursue a doctoral degree in 2019. His dissertation, titled "Process-Property-Structure relationships in advanced rare earth magnet manufacturing: Towards enhanced performance and developing application" was supervised by Dr. Uday Vaidya in the Mechanical, Aerospace and Biomedical Engineering Department. His primary area of research was advanced manufacturing of thermoplastic composites. He conducted his research in collaboration with the Oak Ridge National Lab and Manufacturing Demonstration Facility in Oak Ridge, Tennessee.